BSGF - Earth Sciences Bulletin 2023, 194, 5

https://doi.org/10.1051/bsgf/2022022

Available online at:
www.bsgf.fr

OPEN ACCESS

Parametric mechanical analysis of thin- *versus* thick-skinned tectonics applied to the Jura belt

Typhaine Caër[1], Bertrand Maillot[2,*], Pascale Leturmy[1], Pauline Souloumiac[1] and Christophe Nussbaum[2]

[1] CY Cergy Paris Université, Département Géosciences et Environnement, 95000 Neuville-sur-Oise, France
[2] Federal Office of Topography swisstopo, Wabern, Switzerland

Received: 22 March 2022 / Accepted: 15 December 2022 / Published online: 27 March 2023

Abstract – Field observations and seismic interpretations testify that the front of the Jura fold-and-thrust belt is still submitted to compressive deformation, but whether the basement is deforming (thick-skinned) or not (thin-skinned) is an active question. We propose a mechanical point of view using the Kinematic approach of the Limit Analysis theory (KLA). We first draw cross-sections containing a major shallow décollement level in the Triassic evaporites, including the Alps up to the topographic maximum and including the whole crust. We submit the cross-sections to a compressive force at their southern end, and the KLA determines the location and geometry of the incipient ruptures by optimisation of the associated compressive force, accounting for force balance and for the rock strength (Coulomb criterion). Five cross-sections span the whole Jura from west to east, allowing us to explore the lateral variations. From the analysis of 500 simulations (100 for each cross-section), varying the friction angles of the Triassic décollement and of the lower crust between 1° and 10°, we have identified five types of tectonics at the Jura front depending on the emergence of a basement thrust beyond the Jura front (type 1), at the Jura front (type 2) with simultaneous activation of the shallow décollement (type 3), or south of the Jura front (type 5), with activation of the shallow décollement at the Jura front (type 4). The analysis allows us to draw two conclusions. First, the transitions between the various tectonic styles occur abruptly upon continuous changes in the friction parameters, revealing a threshold behaviour that we interpret as an extension of the concept of wedge criticality in the Critical Coulomb Wedge theory: at criticality, several tectonic types may occur within a narrow, critical range of parameter values. Second, the critical range evolves systematically between cross-sections, in such a way that the front of the thick-skinned deformation crosses laterally the Jura belt. The two most western cross-sections exhibit only thin-skinned or no tectonics at the Jura front (types 1, 4 and 5), the central one hosts all five styles, and the two Eastern ones show thick-skinned solutions (types 1, 2 and 3), for all values tested. We also show that a thick-skinned tectonic style can be accompanied by a simultaneous activation of the shallow Triassic décollement (type 4), complicating the interpretation of apparent thin-skinned field structures. Overall, our simulations yield tectonic styles compatible with natural seismicity and GPS data for values of the lower-crust friction angle below 3 to 7°. Modifications of our cross-sections to explore the effect of a bumpy upper/lower crust interface, or of a major décollement at the upper/lower crust interface, or of higher cohesion values, show that the numerical outcomes are rather robust. They only slightly modify the critical ranges at which the tectonic changes occur. These findings may serve as guides, or first order questions, for more sophisticated mechanical approaches including temperature and rate-dependent rheologies and the three dimensions of space that are necessary to capture the competition between compressive and strike-slip tectonic modes.

Keywords: Jura / fold-and-thrust belt / limit analysis / thick-skinned / thin-skinned / mechanics

Résumé – Analyse mécanique paramétrique de la tectonique pachydermique ou épidermique appliquée à la chaîne du Jura. Observations de terrain et interprétations sismiques témoignent d'une déformation compressive au front de la chaîne de chevauchements–plissements du Jura, mais la question de la distribution de la déformation dans le socle (tectonique pachydermique) ou seulement dans la couverture (tectonique épidermique) reste ouverte. Nous proposons un point de vue mécanique à partir de l'approche

*Corresponding author: bertrand.maillot@cyu.fr

cinématique du calcul à la rupture (CCR). Nous dessinons des coupes avec un décollement majeur dans le Trias, incluant les Alpes jusqu'au maximum topographique, et toute la croûte en profondeur. Ces coupes sont soumises à une compression à leur extrémité sud. La CCR détermine la géométrie des ruptures en vérifiant l'équilibre des forces et la résistance des roches (critère de Coulomb) et en optimisant cette géométrie par rapport à la force de poussée. Cinq coupes balayent le Jura d'Ouest en Est, nous permettant d'explorer les variations latérales. À partir de l'analyse de 500 simulations (100 pour chaque coupe), où nous faisons varier l'angle de friction sur le décollement et l'angle de friction de la croûte inférieure entre 1° et 10°, nous avons défini cinq types de réponse tectonique au front du Jura en fonction de l'émergence d'un chevauchement de socle au-delà du front (type 1), au front (type 2), avec une activation simultanée du décollement triassique (type 3), ou au sud du front (type 5), avec activation du décollement jusqu'au front (type 4). Nous en tirons deux conclusions. D'abord, la transition entre ces différents types tectoniques s'opère brutalement lors d'une variation continue des deux paramètres, révélant ainsi un comportement à seuil que nous interprétons comme une extension du concept de prisme critique de Coulomb : à la criticalité, plusieurs types tectoniques peuvent apparaître dans une gamme très étroite de valeurs des paramètres (quelques degrés). Ensuite, la gamme de valeurs critiques évolue systématiquement entre les coupes, suggérant que le front de la déformation pachydermique traverse latéralement tout le Jura. Les deux coupes les plus à l'Ouest montrent seulement une tectonique épidermique, ou aucune tectonique (types 1, 4, 5), les coupes centrales montrent tous les styles et les deux coupes à l'Est ne montrent que des types pachydermiques (types 1, 2, 3). Nous montrons aussi, plus généralement, que le style pachydermique peut s'accompagner d'une activation du décollement (type 4), compliquant ainsi l'interprétation des marques de tectonique épidermique sur le terrain. Des calculs supplémentaires sur l'effet d'une limite ondulante entre les croûtes supérieure et inférieure, ou sur l'hypothèse d'un décollement majeur entre ces croûtes montrent la robustesse de nos conclusions. Seules les gammes de criticalité changent légèrement. Ces conclusions pourront servir de guide à des analyses plus sophistiquées incluant une rhéologie dépendant du temps et de la température, et une géométrie tri-dimensionnelle pour décrire les régimes tectoniques décrochants.

Mots clés : Jura / chaînes de chevauchement–plissements / calcul à la rupture / pachydermique / épidermique / mécanique

1 Introduction

It is classical in structural geology to describe the deformation style with two different terms, which, according to Pfiffner (2006) and Bauville and Schmalholz (2015), were initially proposed by Rodgers (1949); "thin-skinned tectonics" and "thick-skinned tectonics". The first one refers to a deformation rooted on a shallow décollement located near or at the basis of the sedimentary cover (Chapple, 1978). Only the sediments located above the décollement are affected by the deformation. This term is opposed to "thick-skinned tectonics" which refers to structural styles involving the basement. The definitions of thick-skinned and thin-skinned tectonics differ subtly between authors. Pfiffner (2006), for example, gives more importance to the depth of rooting of the thrusts than to the rheological distinction between basement and sedimentary cover. We use here the definition of Rodgers (1949), broadened by Lacombe and Bellahsen (2016), considering that thick-skinned deformation describes all deformations involving the basement. In that respect, our definition does not follow that of Pfiffner (2016) who uses the term "basement-involved thin-skinned tectonics" to describe the nappe structure in the Alps or elsewhere where thin slivers (100 m to 2 km thick) are thrust on top of each other. We will however distinguish thick-skinned tectonics where the cover is coupled to the basement and thick-skinned tectonics with a simultaneous activation of the shallow décollement as described in the NW Jura front by Madritsch *et al.* (2008). The definition of a basement is not unanimous and depends on the studied area. Hereafter, we focus on the Alpine orogen and more specifically on the Jura fold-and-thrust belt. We consider the Triassic décollement as the limit between the basement and the cover. All the upper crust located below the Triassic décollement is considered here as basement. It is therefore not only composed of crystalline material but also of Permo-Carboniferous and lower Triassic (Buntstandstein) sediments. It is generally accepted that the Jura belt was emplaced in Mio-Pliocene times in a thin-skinned tectonic style using the shallow Triassic décollement, but it is suspected to be currently affected by thick-skinned tectonics, *i.e.*, deformation below the Triassic sediments (Mosar, 1999; Becker, 2000; Giamboni *et al.*, 2004; Ustaszewski *et al.*, 2005; Pfiffner, 2006; Ustaszewski and Schmid, 2006, 2007; Madritsch *et al.*, 2008, 2010; Pfiffner, 2014; Lacombe and Bellahsen, 2016).

This study gives a mechanical point of view to the above geological interpretation, making use of the theory of Limit Analysis. This theory offers a natural generalisation of Dahlen's Critical Coulomb Wedge theory (Dahlen, 1984) to predict the geometry of failure in more complex prototypes including rheological heterogeneities, inherited faults and surface processes (Maillot and Leroy, 2006; Cubas *et al.*, 2008; Souloumiac, 2009; Mary, 2012; Mary *et al.*, 2013a, 2013b). It is a simple approach limited to frictional behaviours and, in its current implementation, limited to the onset of plastic deformation. There are many numerical approaches solving the full physical problem and the time evolution at the lithosperic scale (*e.g.*, Jammes and Huismans, 2012; Jammes *et al.*, 2014; Ruh *et al.*, 2015) but they cannot address the details of the shallow Triassic décollement and the formation of the Jura. There are also several numerical mechanical studies of tectonics above a pre-defined décollement, using viscous or frictional formulations, or a combination of them (*e.g.*, Strayer *et al.*, 2001; Wissing *et al.*, 2003; Buiter *et al.*, 2006;

Jaquet *et al.*, 2014; Bauville and Schmalholz, 2015; Buiter *et al.*, 2016; Humair *et al.*, 2020). Here, our goal is to capture the spontaneous occurrence of thick-skinned tectonics in the context of the Jura by considering a very large region around the Jura belt to minimize the effects of the boundary conditions, and to perform hundreds of tests so as to draw robust conclusions. However, the depth of the cross-sections we will consider overcomes the frictional-ductile transition and, in that respect, the frictional formulation is really a proxy for a more complex ductile, temperature and rate-dependent rheology.

The contents are as follows. In Section 2, we redraw, or construct, five cross-sections spanning the whole Jura, assuming the presence of potential décollements in the Trias (D_1). In Section 3, we construct five mechanical prototypes by populating the cross-sections with mechanical properties and applying a compressive force at their southern ends. In Section 4, we conduct a parametric study of the friction angles of D_1 and of the lower-crust, and we classify the various solutions in terms of thick- or thin-skinned styles. Section 5 concludes on the current tectonic style varying from West to East. We also test and discuss the validity of various assumptions made when designing the prototypes, and propose the concept of a critical state in the sense of the Critical Coulomb Wedge theory (Dahlen, 1984).

2 Tectonics settings

2.1 Emplacement of the Jura fold-and-thrust belt

The Jura fold-and-thrust belt is an arcuate mountain range formed between Serravalian times and early Pliocene times (Laubscher, 1992; Becker, 2000; Nussbaum *et al.*, 2018) and represents the northern part of the Alpine orogeny. It formed in an area presenting an extensive inheritance resulting from the Permo-Carboniferous extension that forms ENE to NE grabens below the actual northern Jura, and the Oligocene extension responsible for the opening of the Rhine and Bresse grabens, which currently frame the Jura belt. The northern part of the Jura was formed along the resulting Rhine-Bresse transfer zone (RBTZ) (Nussbaum *et al.*, 2018), which played the role of corridor with both extensive and strike-slip deformation, probably reactivating Permo-Carboniferous normal faults. Despite this extensive heritage, the Jura fold-and-thrust belt is commonly presented as the archetype of a thin-skinned fold-and-thrust belt formed by the activation of the evaporitic Triassic layers as a décollement (Buxtorf, 1916; Laubscher, 1961; Burkhard, 1990; Burkhard and Sommaruga, 1998; Pfiffner, 2006; Madritsch *et al.*, 2008, 2010). The inherited faults are considered to have influenced the thin-skinned deformation by localizing the ramps (Ustaszewski and Schmid, 2007; Caër *et al.*, 2018; Schori, 2021; Schori *et al.*, 2021).

2.2 The current tectonics of the Jura fold-and-thrust belt

Some authors mention the involvement of the basement in certain structures by the reactivation of the older normal faults (Guellec *et al.*, 1990; Pfiffner *et al.*, 1997; Rotstein and Schaming, 2004; Ustaszewski and Schmid, 2007; Madritsch *et al.*, 2008, 2010), and this is associated to a late (post-tardi-Pliocene) development of a thick-skinned tectonics in the Jura (Becker, 2000; Giamboni *et al.*, 2004; Ustaszewski *et al.*, 2005; Ustaszewski and Schmid, 2007; Madritsch *et al.*, 2008). Seismicity studies (Deichmann *et al.*, 2000; Kastrup *et al.*, 2004) and geomorphological studies (Dreyfuss and Glangeaud, 1950; Giamboni *et al.*, 2004; Madritsch, 2008; Madritsch *et al.*, 2008) show that the Jura fold-and-thrust belt is still submitted to deformation. The deformation rates are very low and it is thus difficult to determine the source depth and the focal mechanisms, and therefore the tectonic style (Meyer *et al.*, 1994; Nivière and Winter, 2000; Meghraoui *et al.*, 2001; Giamboni *et al.*, 2004; Ferry *et al.*, 2005; Lambert *et al.*, 2005; Ustaszewski and Schmid, 2007; Madritsch *et al.*, 2010). Field observations and seismic interpretations give arguments for basement deformation (Becker, 2000; Rotstein and Schaming, 2004; Giamboni *et al.*, 2004; Ustaszewski *et al.*, 2005; Ustaszewski and Schmid, 2007; Madritsch *et al.*, 2008, 2010), but also for a deformation of the sedimentary cover along the Triassic décollement. The anticlines deforming the Pliocene "Sundgau gravels" have orientations that can be linked to the reactivation of basement faults (Giamboni *et al.*, 2004; Ustaszewski and Schmid, 2007). In the Saint-Ursanne area (Central-northern front of the Jura), the 2000 earthquake sequence has been reevaluated as resulting from shallow, probably back-thrusting activity above the Triassic décollement (Lanza *et al.*, 2022).

Most of the arguments for basement involvement in the deformation come from the Northeastern front of the belt, where the seismicity is abundant at depths greater than 15 km (Rabin *et al.*, 2018). In the south of the belt, the seismicity is scarce and the current deformation is unclear, with descriptions of both compressive and extensive structures (Jouanne *et al.*, 1994; Baize *et al.*, 2002; De La Taille, 2015). Compiling extensive seismic and geodesy data sets, Rabin *et al.* (2018) conclude on basement–cover decoupling in the NE part of the belt, and coupling in the western part, and beyond all the Jura front. They further observe a NW–SE gradient of uplift, from no uplift at the Jura front to about 0.4 mm/yr at the Alpine front.

Concerning the stress state, throughout the belt, focal mechanisms point to a strike-slip to thrusting mode with a more or less radial azimuth evolving from WNW–ESE compression in the west and south of the belt to NNW–SSE in the east (Kastrup *et al.*, 2004; Rabin *et al.*, 2018; Radaideh and Mosar, 2021). This strike-slip mode, involving the basement by reactivation of Permo-Carboniferous troughs, is interpreted by Mock and Herwegh (2017) as a transition toward a thrusting mode delaminating the crust up to the Molasse basin and the Jura belt, after the detachment of the subducting European mantle. However, in the Saint-Ursanne area, the stress state above the depth of 5 km is in NNW–SSE compression, and changes to strike-slip to extension at depths between 5 and 15 km (Lanza *et al.*, 2022).

These findings and interpretations are at the base of our mechanical analysis, which will aim at determining the values of the rheological parameters that are compatible with their major features. We first draw, or redraw, five cross-sections.

2.3 Five regional cross-sections

We consider five cross-sections scanning laterally the whole Jura, from the Alps to the Jura foreland, as prototypes for our mechanical modeling (Figs. 1 and 2). The southern

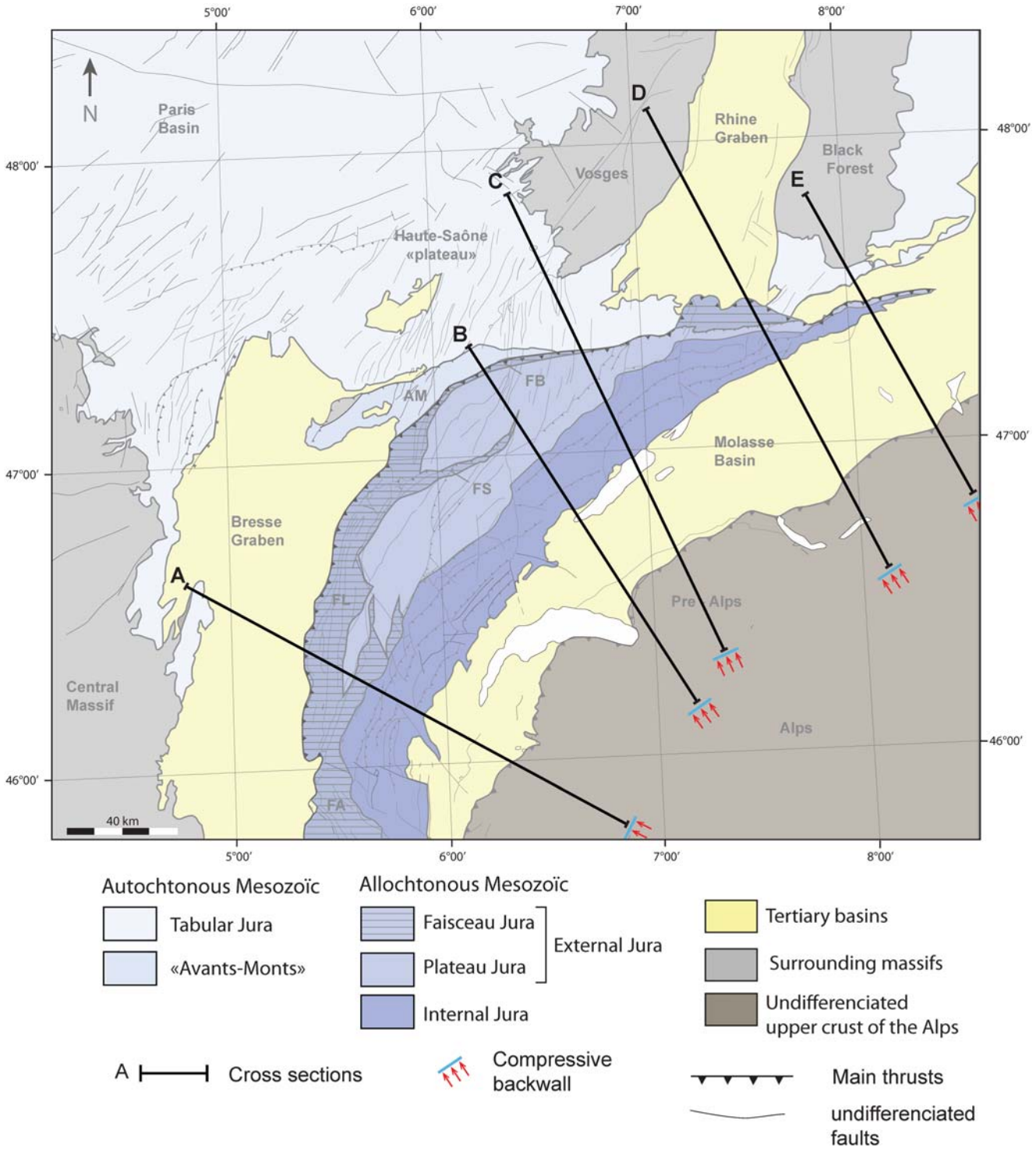

Fig. 1. Geological map of the Jura and its surroundings and position of the five cross-sections used as prototypes in this study. The symbol with red arrows represents the compression applied in the mechanical analysis of each prototype. FB: "Faisceau Bisontin"; FS: "Faisceau Salinois"; FL: "Faisceau du Lomont".

most one, cross-section A, corresponds to the ECORS profile, redrawn after Schmid and Kissling (2000) and Philippe (1995) (Fig. 2). Northward, the cross-section B has been redrawn after Burkhard and Sommaruga (1998). Cross-sections C, D and E have been realized for this study based on the data of Pfiffner *et al.* (1997), Sommaruga (1999), Rotstein *et al.* (2006), Ustaszewski and Schmid (2007) and Sommaruga *et al.* (2012). These cross-sections overtake widely the Jura belt in order to minimize the impact of the boundary conditions used in the mechanical prototypes, and to better account for the effects of the neighboring regions.

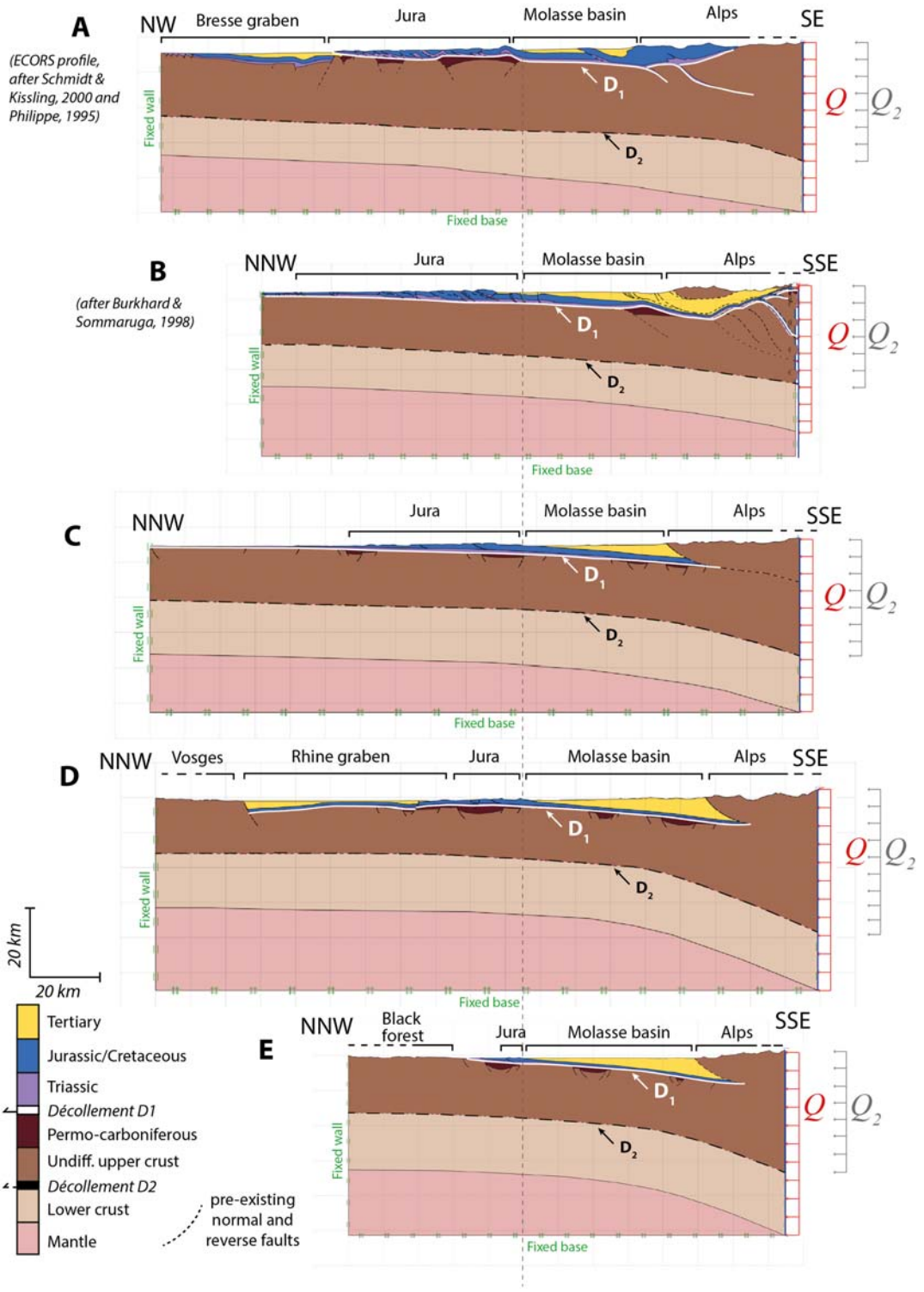

Fig. 2. The five cross-sections used as mechanical prototypes. Cross-section A corresponds to the ECORS profile, redrawn after Schmid and Kissling (2000) and Philippe (1995). Cross-section B has been redrawn after Burkhard and Sommaruga (1998), and cross-sections C, D and E are original, based on Pfiffner *et al.* (1990), Sommaruga (1999), Rotstein *et al.* (2006), Ustaszewski and Schmid (2007) and Sommaruga *et al.* (2012). The cross-sections are aligned along the vertical dashed line showing the limit between the Jura and the Molasse basin. The mechanical properties of each material are presented in Table 1. A horizontal compressive force Q is applied on the crust along the southern wall (red arrows). The vertical fixed wall with green dashed lines on the left precludes any horizontal movement and allows any vertical movement. The fixed base, with green hash signs, precludes any horizontal and vertical movements. We also consider an alternative prototype where the force (Q_2) is applied on the upper crust only, and where we introduce a detachment D_2 between the upper and lower crusts.

We can distinguish four different structural domains. The northern one corresponds to the foreland and is represented by the Bresse graben on cross-section A, the Haute-Saône plateau on cross-sections B and C, the Rhine graben and the Vosges on cross-section D and the Black Forest massif on cross-section E. The second domain, to the south-east corresponds to the Jura fold-and-thrust belt and its width increases from 0 km close to Basel in the Northeastern Jura to more than 50 km on cross-section B to the south-west and decrease again to the south on cross-section A. To the south-east, the strongly deformed Jura domain is separated from the Alps by the little deformed flexural Miocene Molasse basin filled by erosion products coming from the Alps.

The Cenozoic part of the sedimentary cover is represented by the Tertiary infilling of the Molasse basin and of the Rhine and Bresse grabens. The thickness of the underlying Mesozoic cover evolves from 1 km to the north of our cross-sections to 3 km in the south (Nussbaum *et al.*, 2011) and is essentially composed of Triassic evaporites and Jurassic limestones. Cretaceous sediments are well developed in the internal Jura, less developed to the north and absent to the east due to a heterogeneous sedimentation process (Homberg, 1997). Since we use our cross-sections as prototypes for the mechanical modeling, we chose to simplify the stratigraphy by merging the Cretaceous and Jurassic sediments in a single mechanical layer.

Below the Molasse basin and the Jura fold-and-thrust belt, the basement is composed of medium to high grade metamorphic and plutonic rocks deformed during the Variscan orogeny, and it is affected by Permo-Carboniferous grabens filled by sediments (Sommaruga, 1997). These sediments constitute the Permo-Carboniferous unit of our cross-sections. We choose to model the Alpine domain and the remainder of the upper crust as a uniform domain with only one material labelled "undifferentiated upper crust" (Fig. 2). We also consider a unique material for the lower crust, and another one for the mantle.

In this stratigraphic pile, the Triassic décollement, named hereafter "D_1", is responsible of the Jura folding, and is located in the Keuper gypsum in the southwest Jura, and in the Muschelkalk evaporites in the northeast (Mugnier and Vialon, 1986; Jordan, 1992). This décollement is slightly dipping (1° to 3°) toward the hinterland (Sommaruga, 1999; Mosar, 1999). On cross-section A, the surface of the décollement presents a bump below the internal part of the Jura and we assume that it is due to the reactivation of a Permian graben as proposed by Philippe (1995) and Pfiffner (2006, 2014), which is also the hypothesis adopted by Burkhard and Sommaruga (1998) on the cross-section B to explain a bump below the Molasse basin (Fig. 2).

In cross-sections C, D and E, we consider that the upper-lower crust limit, labelled D_2 in Figure 2, is at 15 km below the Jura (Mosar, 1999; Schmid and Kissling, 2000), and we prolonged it below the Alps assuming regional isostasy. Note that in the west and east ends of the Jura, Pfiffner (2014, 2016) draws an irregular upper-lower crust limit, undulating at wavelengths of 20 to 40 km with an amplitude of 7 to 10 km. However, in the absence of equivalent data for the other cross-sections, we prefer not to account for these variations in our mechanical analysis, although we propose some additional simulations of cross-section A accounting for this undulation in the final section.

Another simplification made in these cross-sections is the absence of a décollement zone within the upper crust, on which the Permo-Carboniferous grabens would root, and which would be reactivated to produce the recent basement deformations. Such a décollement has been inferred at 1 to 3 km below the Triassic décollement under the Molasse basin (Pfiffner *et al.*, 1997) but it has not been directly detected nor quantitatively inferred below the Jura. For this reason, we prefer to avoid drawing a pre-defined décollement and let the mechanical modelling find a solution. We however propose some additional simulations accounting for this potential décollement in cross-section C in the final section.

3 Mechanical modelling of the Jura tectonics

3.1 Method

We use the kinematic approach of limit analysis (Salençon, 2002) to determine the potential zones of failure due to the compressive force Q applied on the southern ends of the cross-sections (Fig. 2). The general procedure is: (i) to set up a prototype with mechanical properties (Coulomb parameters and volumic mass) and with boundary conditions including the boundary of application of the compressive force, its direction, but not its magnitude, which will remain unknown; (ii) to determine a failure mode (*i.e.*, a velocity field) that is compatible with the boundary conditions, the force balance, and the finite rock strength defined by the Coulomb criterion; (iii) to optimize the failure mode with respect to the applied compressive force so that the optimal velocity field corresponds to the lowest possible value of the compressive force. This value is called the lowest upper bound, meaning that the actual compression force required to reach plastic deformation (according to the Coulomb criterion) is necessarily lower or equal to that value. Note that elastic parameters are not required: the elastic deformations at the onset of plastic failure are disregarded.

Previous uses of this method for kink folding (Maillot and Leroy, 2006) and for frontal accretion (Cubas *et al.*, 2008; Mary, 2012; Mary *et al.*, 2013a, 2013b) describe all details of semi-analytical implementations. Here, we only give the general equations and present briefly the numerical implementation. We first write the static force balance in its weak, or integral, form using the theorem of virtual powers. Noting $\hat{\underline{V}}$ a virtual velocity field defined over the domain Ω (representing the cross-section) that is kinematically acceptable (meaning that $\hat{\underline{V}}$ is piece wise continuous and that it obeys the boundary conditions), we define the internal power:

$$P_{\text{int}}\left(\hat{\underline{V}}\right) = \int_{\Omega} \underline{\underline{\sigma}} : \underline{\underline{d}}\left(\hat{\underline{V}}\right) dV + \int_{\Sigma_V} \underline{T} \cdot [\![\hat{\underline{V}}]\!]\, dS, \qquad (1)$$

where $\underline{\underline{\sigma}}$ is the stress tensor, $\underline{\underline{d}}\left(\hat{\underline{V}}\right)$ is the rate of deformation tensor, Σ_V denotes the internal surfaces across which the velocity is discontinuous, $\underline{T}$, the traction vector across these discontinuities, and $[\![\hat{\underline{V}}]\!]$, the velocity difference between each side of the discontinuities. Note that this explicit account of discontinuities is a specific feature of the limit analysis that is particularly useful to account for faults in geological applications.

Table 1. Values used for the parametric study (a few other values were tested in the Section 5).

Parameters of the prototypes	ϕ (°)	c (MPa)	ϕ_F (°)	c_F (MPa)	ρ (kg/m^2)
Tertiary	10	1	10	0	2700
Jurassic/Cretaceous	30	1	15	0	2700
Triassic	10	1.2	10	0	2700
Décollement D_1	[1–10]	0	–	–	–
Permo-Carboniferous	20	1	15	0	2700
Undifferenciated upper crust	30	1.5	15	0	2700
Lower crust	[1–10]	1	–	–	2700
Mantle	30	1	–	–	3000

The external power:

$$P_{\text{ext}}(\hat{\underline{V}}) = \int_{\Omega} \rho \underline{g} \cdot \hat{\underline{V}}\, dV + \alpha \int_{\partial\Omega_Q} \underline{Q}^o \cdot \hat{\underline{V}}\, dS, \tag{2}$$

is the sum of the power of the gravity $\underline{g}$ (ρ denotes the volumic mass) and the power of the tectonic compressive force $\alpha\underline{Q}^o$ applied on $\partial\Omega_Q$ (representing the southern vertical end wall of our cross-sections). $\underline{Q}^o$ is a horizontal vector field defined on $\partial\Omega_Q$ of unit norm and the magnitude of the compression is thus α, measured in Pa.

The theorem of virtual powers, expressing the force balance in an integral form, reads:

$$P_{\text{ext}}(\hat{\underline{V}}) = P_{\text{int}}(\hat{\underline{V}}) \text{ for all fields } \hat{\underline{V}}. \tag{3}$$

In classical finite-element simulations, we would now add equations describing the rheology (elasticity, a plasticity criterion, and a plastic flow rule), and proceed with the discretisation of the equations and their resolution through space and time to obtain approximate solutions of the stress and velocity fields. The kinematic approach of limit analysis solves a simpler problem by replacing the internal power by an upper bound calculated with the help of a support function denoted π and defined as:

$$\pi(\underline{\underline{d}}(\hat{\underline{V}})) = \text{Sup}\left\{ \underline{\underline{\sigma}} \ : \underline{\underline{d}}(\hat{\underline{V}}) \text{ such that } \underline{\underline{\sigma}} \in G \right\}, \tag{4}$$

and:

$$\pi(\llbracket \hat{\underline{V}} \rrbracket) = \text{Sup}\left\{ \underline{T} \cdot \llbracket \hat{\underline{V}} \rrbracket \text{ such that } \underline{T} \in G \right\}, \tag{5}$$

where G is the strength domain, corresponding in this paper to the Coulomb criterion. The existence of the support function is a result of the convexity of the strength domain and its calculation may be found in Salençon (1974). An explicit calculation of $\pi(\llbracket \hat{\underline{V}} \rrbracket)$ for the Coulomb criterion may be found in Maillot and Leroy (2006). With these definitions, we can remove all mentions of the stress field in the theorem of virtual powers (eq. (3)) to obtain:

$$P_{\text{ext}}(\hat{\underline{V}}) \leq \int_{\Omega} \pi(\underline{\underline{d}}(\hat{\underline{V}}))dV + \int_{\Sigma_V} \pi(\llbracket \hat{\underline{V}} \rrbracket)dS, \text{ for all fields } \hat{\underline{V}}. \tag{6}$$

Replacing $P_{\text{ext}}(\hat{\underline{V}})$ by its definition (eq. (2)), we obtain:

$$\alpha \leq \frac{\int_{\Omega} \pi(\underline{\underline{d}}(\hat{\underline{V}}))dV + \int_{\Sigma_V} \pi(\llbracket \hat{\underline{V}} \rrbracket)dS - \int_{\Omega} \rho \underline{g} \cdot \hat{\underline{V}}\, dV}{\int_{\partial\Omega_Q} \underline{Q}^o \cdot \hat{\underline{V}}\, dS}, \quad \text{for all fields } \hat{\underline{V}}. \tag{7}$$

The steps (ii) and (iii) mentioned at the beginning of this section use the Equation (7). We use the software Optum G2 (Krabbenhøft and Lyamin, 2014), based on the theoretical and numerical developments of Krabbenhøft and Damkilde (2003), Krabbenhøft *et al.* (2005), Lyamin *et al.* (2005) and Souloumiac *et al.* (2009, 2010). The velocity field $\hat{V}$ is discretised using a Voronoi mesh that is automatically refined in zones of high gradients. In addition, special zero-thickness elements allow the velocities to be discontinuous, and that is accounted for by the Equation (5). Fault planes can thus be described as true discontinuities. The optimisation problem consists in finding the velocity field $\underline{V}$ that minimises the right hand side of Equation (7). In the following, our numerical outcomes are all presented in terms of this optimised velocity field and we neither present nor use further the upper bound value of α.

3.2 Prototypes

The prototypes are the five cross-sections enriched with boundary conditions (Fig. 2) and with material parameters (Tab. 1). The Northern vertical walls with two parallel green dashed lines (labelled “Fixed wall”) block any horizontal movement while vertical movements meet no resistance. The basis is fixed (labelled “Fixed base”), *i.e.* precluding any movement. A compressive force Q is applied on the southern end of the cross-sections (red arrows in Fig. 2). The hypothesis that the Jura fold-and-thrust belt is currently submitted to compressive deformation is supported by focal mechanisms and paleotectonic studies, which indicate a general NW–SE direction of compression throughout the region and even beyond, to the North and West of the Bresse and Rhine grabens respectively, as recently summarised by Radaideh and Mosar (2021). In the south-west of the Jura, the compression is slightly rotated towards the west, trending WNW–ESE (Kastrup *et al.*, 2004; Rabin *et al.*, 2018). The main compression is therefore more or less parallel to each of our cross-sections. We chose to place the compressive wall at the

first high summit in the Alps, before the occurrence of a deep valley further to the South-east. In most of our results, the deformation occurs in the middle of the cross-sections and does not reach the southern end because the area of the Alps forms a stable prism. Therefore, the exact position of the compressive wall has little influence on the results. However, and obviously, the two-dimensional nature of our calculations on vertical cross-sections does not allow us to account for strike-slip faulting: all compression results in reverse faulting striking perpendicular to the cross-sections.

There are three material parameters to define for each rock type (the friction angle ϕ, the cohesion c, and the volumic mass ρ, see Tab. 1). We attribute a friction angle of 30° to all the competent layers (the Jurassic/Cretaceous unit, the undifferentiated upper crust unit and the mantle), and a value of 10° to the most incompetent layers (Tertiary and Triassic units). In the Permo-Carboniferous sediments in the grabens, we consider an intermediary friction angle of 20°. The cohesion cannot be neglected, because it is necessary to avoid gravitational collapses at the surface, which are detected by the software Optum G2. By trial and error, we obtained 1 MPa in the Tertiary unit and the Jurassic and Cretaceous units, 1.2 MPa in the Triassic unit and 1.5 MPa in the upper crust unit. For the units that do not outcrop (the Permo-Carboniferous unit, the lower crust and the mantle), we choose to set a cohesion of 1 MPa, to be in the same range of cohesion as that of the above units. Higher values of the cohesion, at 5 and 10 MPa are tested in the Section 5.

For the pre-existing faults, *i.e.* those drawn in the cross-sections, we consider that the part of the faults that cross competent layers (Jurassic/Cretaceous and upper crust undifferentiated) is softened, *i.e.*, their friction (ϕ_F) is lower than the one of the surrounding material and their cohesion $c_F = 0$ MPa.

Finally, we set a volumic mass of 2700 kg/m^2 in all the crust, and 3000 kg/m^2 in the mantle. The décollements D_1 has no thickness and thus no volumic mass is given in Table 1.

The Triassic salt and the lower crust are known to be partially viscous and this cannot be directly accounted for in limit analysis. To determine the values of the friction angle that could mimic the viscous behaviour of the salt, we first estimate the shear stress (τ_{basal}) at the base of the sedimentary pile above the Triassic décollement with the hypothesis of a Couette flow (or simple shear) in the décollement:

$$\tau_{basal} = \mu_{Trias} * \frac{V_{max}}{e_{Trias}}, \tag{8}$$

where μ_{Trias} is the viscosity, V_{max} the slip velocity above the décollement, and e_{Trias} the thickness. Second, the Coulomb parameters: ϕ_{D_1} and c_{D_1} that produce the same shear stress must obey:

$$\tau_{basal} = \tan\phi_{D_1}\,\sigma_n + c_{D_1}. \tag{9}$$

Next, since the décollement D_1 is sub-horizontal, the normal stress acting on it is:

$$\sigma_n = \rho * e_{sed} * g, \tag{10}$$

where e_{sed} is the thickness of the sedimentary pile above the décollement. This yields an infinity of solutions, from which we retain:

$$\tan\phi_{D_1} = \mu_{Trias} * \frac{V_{max}}{e_{Trias}\,\rho e_{sed}\,g}, \text{ and } c_{D_1} = 0. \tag{11}$$

Estimating the viscosity $\mu_{Trias} = 10^{18}$ Pa.s (Costa and Vendeville, 2002), the shortening velocity $V_{max} = 5$ mm/a (25 km of shortening between 9 and 4 Ma (Becker, 2000), the décollement thickness $0 < e_{Trias} \leq 1000$ m (Sommaruga, 1999; Affolter and Gratier, 2004; Schori, 2021), the thickness of the sediments above the décollement $e_{sed} = 1500$ to 3000 m, and the gravity $g = 9.81$ m/s^2, we obtain from Equation (11);

$$\phi_{D_1} \leq 20°, \text{ for } c_{D_1} = 0 \text{ MPa}. \tag{12}$$

These low values mimic the viscous behaviour of the décollement D_1 that is not much sensitive to pressure because of the high content in evaporites and clays. However, we restrict the range to $1° \leq \phi_{D_1} \leq 10°$ on the décollement because, beyond this range, only minor changes occur that do not modify our conclusions. For the same reason, we let the friction angle of the lower crust vary in the same range: $1 \leq \phi_{LC} \leq 10°$.

Note, finally, that the assumption of a purely plastic/frictional deformation is not incompatible with the existence of folds in the Jura belt. Mary *et al.* (2013b) have shown that an incremental succession of ruptures along a fore thrust and its associated back thrust using the same theoretical approach of limit analysis leads to a great variety of finite structures, including anticlines, fault propagation folds and fault-bend folds, essentially depending on the amount of frictional weakening during deformation. The missing feature when adopting a frictional only behaviour is the rate sensitivity that comes from a viscous behaviour. Since we perform only calculations of the onset of deformation, without integrating through time, it is sufficient to produce a stress state equivalent to the stress state in a viscous material, as we did with Equations (8–12).

4 Parametric study of the friction angles of the Triassic décollement D_1 and of the lower crust

4.1 Identification of tectonic styles

We made 500 simulations varying the friction angles between 1° and 10° by increments of 1° on the décollement ϕ_{D_1} and in the lower crust ϕ_{LC} (Tab. 1). That is 100 simulation for each of the five prototypes. Each result is unique, but we can group them by common features. We focus on the frontal part of the Jura (the 25 km wide area, represented by a black dashed rectangle on Fig. 3), and we group the results by common tectonic style in this area. The Figure 3 illustrates the five different types of results that we identified, using examples of cross-section C. These results are presented as cross-sections of the norm of the velocity vector at the onset of failure, denoted |U|, with fastest moving regions in red, and immobile

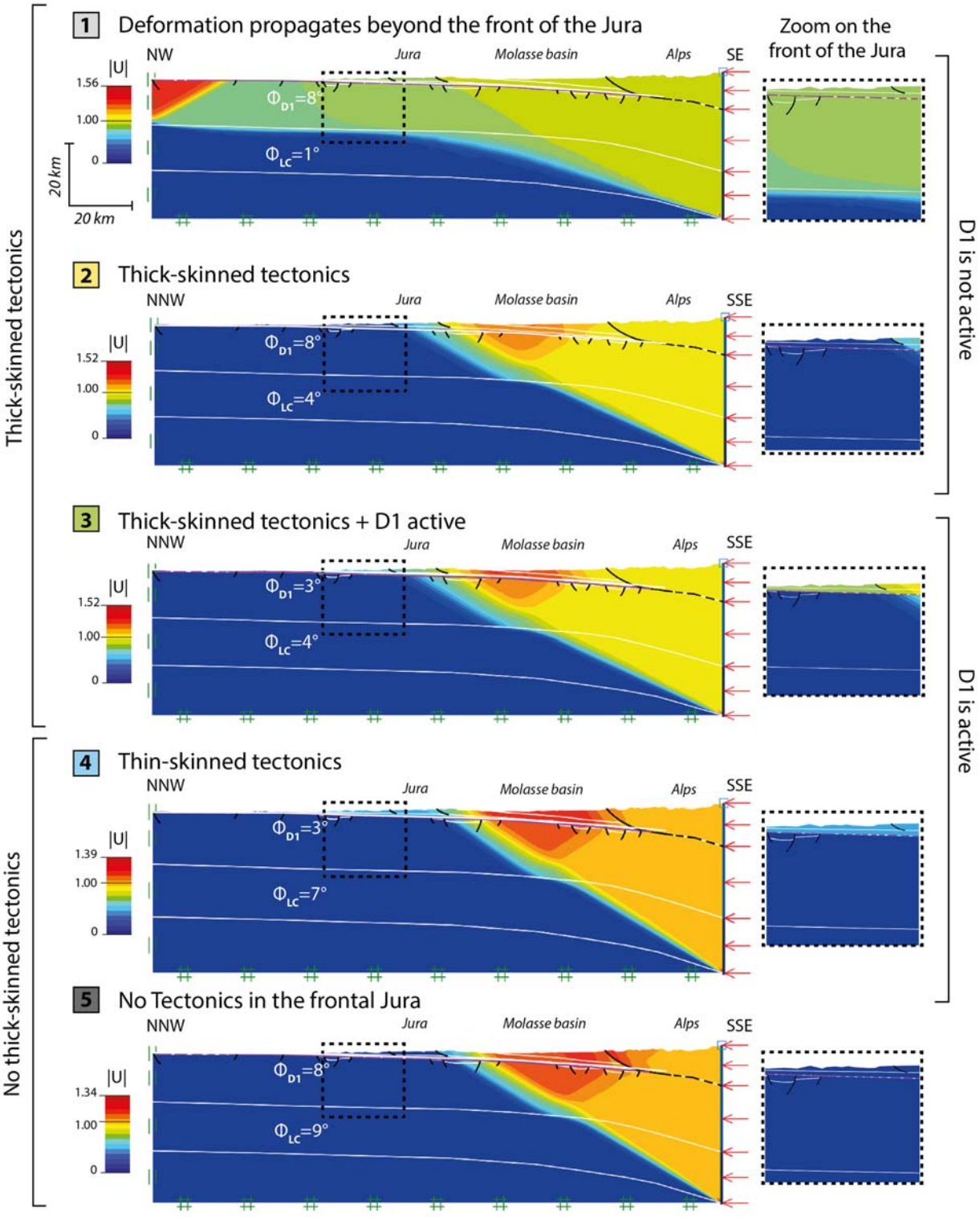

Fig. 3. Examples of limit analysis results using Optum G2 from prototype C, classified by tectonic style in the frontal Jura (black dashed rectangle). Colours show the absolute value of the velocity vector |U| normalised by the horizontal component of the velocity at the pushing wall (red arrows). Type 1 groups results in which the deformation propagates beyond the front of the Jura. In type 2, the Jura front is submitted to pure thick-skinned tectonics, in type 3, the tectonic is thick-skinned but the Triassic décollement D_1 is active too, in type 4, the Jura front undergoes thin-skinned tectonics, and, in type 5, the Jura front is not affected by the deformation.

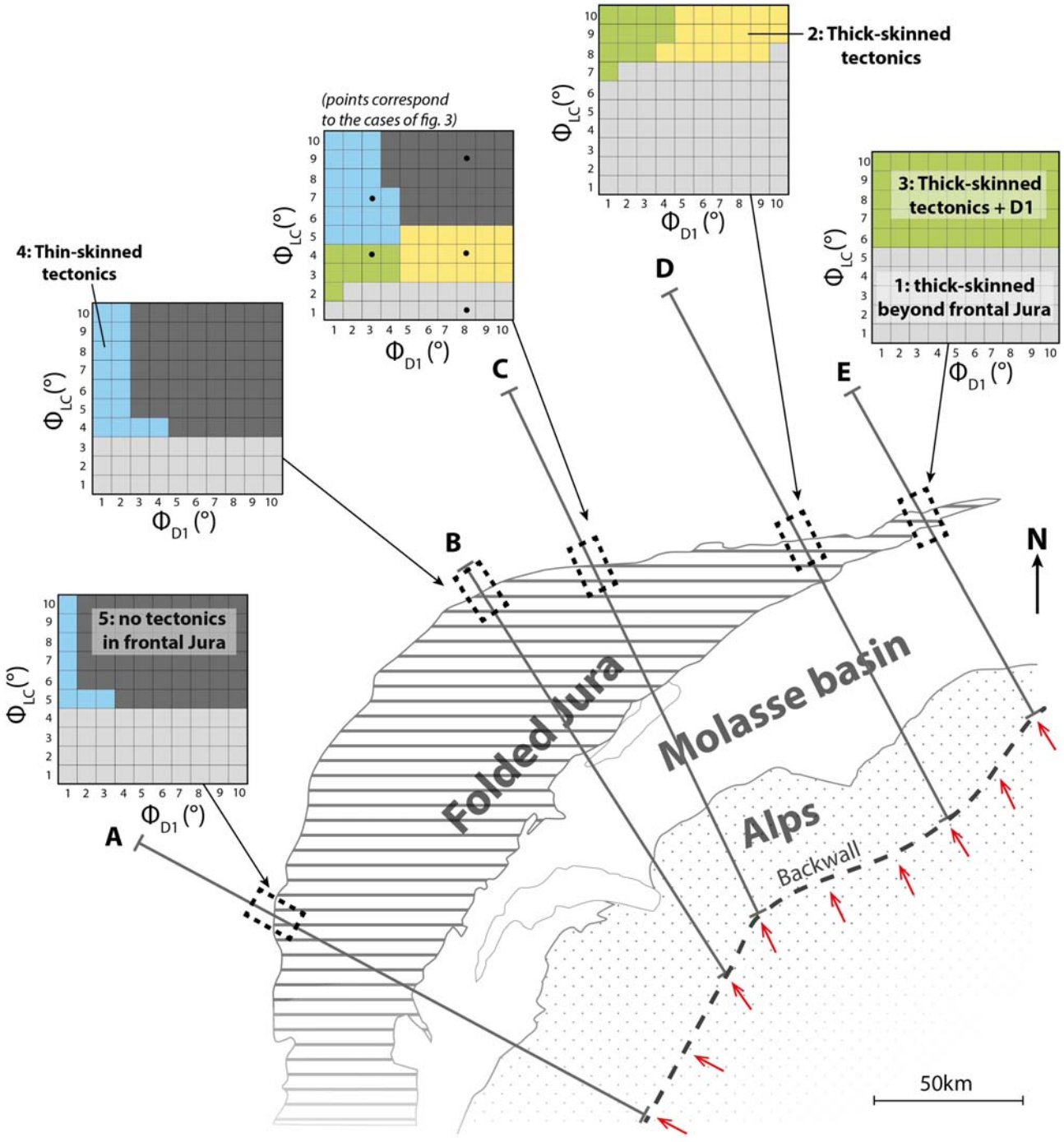

Fig. 4. Tectonic styles affecting the frontal part of the Jura (dashed rectangles) as functions of the Triassic décollement friction angle ϕ_{D_1} and of the lower crust friction angle ϕ_{LC}. In the South, on cross-section A, the tectonics is either inactive (dark grey), thin-skinned (blue) or reaching beyond the Jura front (light grey). Towards the North-East, the Jura evolves to a thick-skinned style on cross-sections D and E, activating the Triassic décollement (green) or not (yellow). On cross-sections B and C, both thin- or thick-skinned tectonics are possible (black dots in the graph C correspond to the examples of Fig. 3). These results suggest that a thick-skinned front cross-cuts the Jura belt (see Fig. 5).

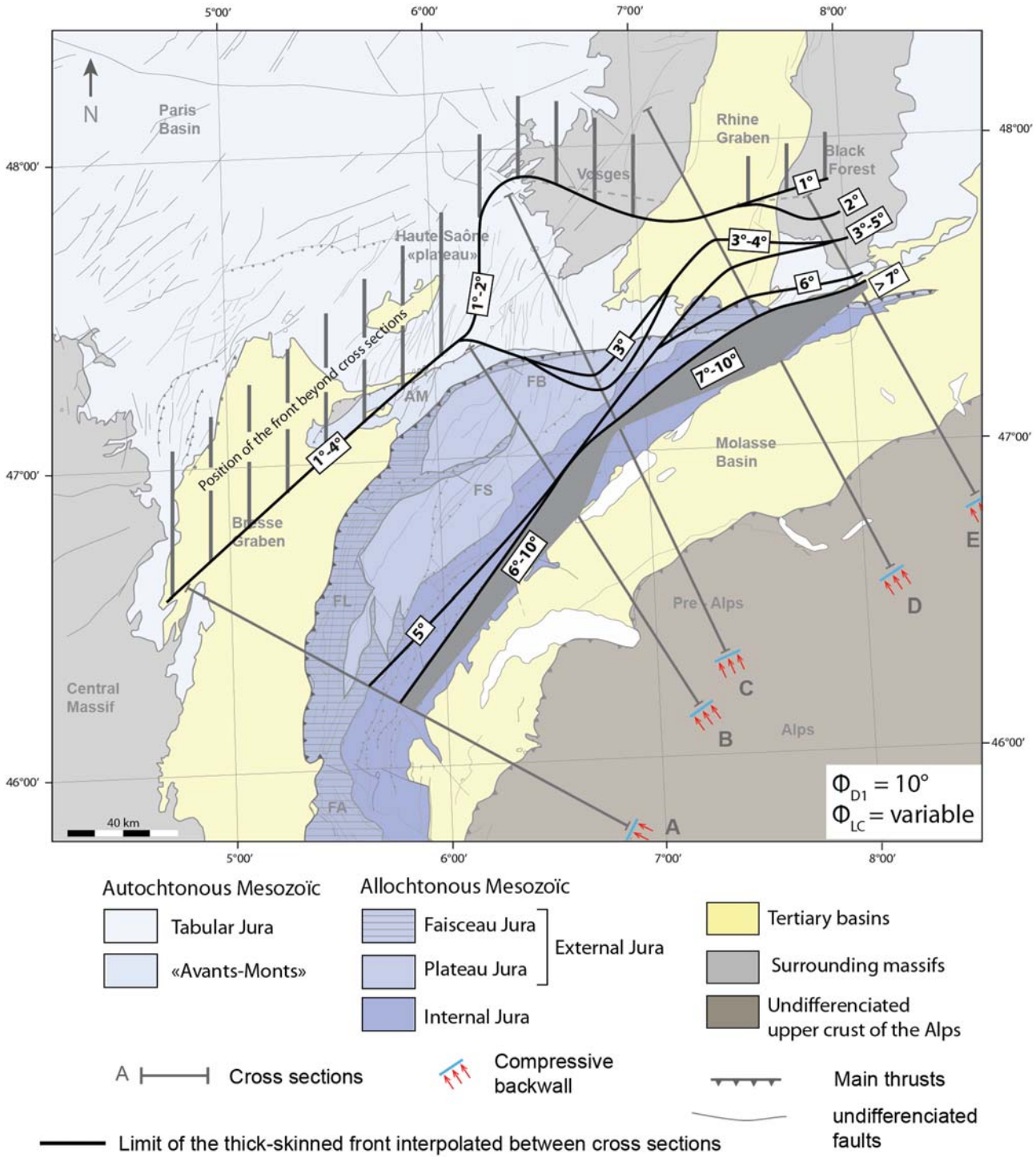

Fig. 5. Position of the front of the thick-skinned deformation for different values of friction in the lower crust (ϕ_{LC}). The Triassic décollement is blocked by setting $\phi_{D_1} = 10°$.

regions in blue. The displayed numerical values of |U| in the colour bars have been normalised by the horizontal component of the velocity at the rigid pushing wall. In the figures, $|U| > 1$ mostly indicate regions with a substantial component of vertical movement. Zones of high color gradient correspond to zones of high strain rates, indicating sharp localisation. This occurs in the lower crust as a straight ramp dipping more steeply as ϕ_{LC} is increased from type 1 to type 5 (top to bottom of Fig. 3). In the upper crust, newly formed ramps and back thrusts rooted on the lower crust ramp reach the surface triggering various tectonic types.

In type nr. 1 (light grey) the deformation propagates so far that the crustal ramp emerges beyond the Jura front and, in most of cases, reach the northern fixed wall. This implies thick-skinned deformation beyond the limit of the folded Jura towards the North and West. In type nr. 2 (yellow), the crustal

ramp emerges in the frontal part of the Jura without any activation of D_1, corresponding to thick-skinned tectonics. The type nr. 3 (green) is similar to type nr. 2 but with a simultaneous activation of D_1 that is clearly visible in the associated zoom image to the right. Note that these three tectonic styles are reminiscent of the proposition of Mosar (1999) that there is an incipient basement imbricate in the Molasse basin and central Jura regions formed by tectonic underplating. The proposed mechanical explanation uses the theory of the Critical Coulomb Wedge and, in that respect, it is qualitatively similar to our analysis. In type nr. 4 (blue), the frontal part of the Jura undergoes thin-skinned tectonics: D_1 is active, but the crustal ramp emerges south of the frontal part of the Jura. Because D_1 is active, there is mechanical decoupling between basement and cover in types 3 and 4, while they are coupled in types 1 and 2. In type 5 (dark grey), the crustal ramp emerges near the limit between the Jura and the Molasse basin, or in the Molasse basin, and the frontal part of the Jura remains undeformed.

An interesting general outcome is that for a certain set of parameters, the shallow décollement can be activated simultaneously with basement deformation. It results in a thick-skinned tectonics associated to some apparent thin-skinned deformation. Therefore, a field observation of a structure rooted on a shallow décollement cannot be interpreted as a proof of an ongoing thin-skinned tectonics and, in the same way, a thick-skinned tectonic activity does not mean that a shallow décollement, if present, is blocked. This simultaneous activity could explain the variety of observations in favor of both thick- and thin-skinned tectonics in the Jura mentioned by Madritsch *et al.* (2010).

4.2 Distribution of tectonic styles throughout the Jura belt

The results of the parametric study are presented on five graphs (Fig. 4) with ϕ_{D_1} on the horizontal axis and ϕ_{LC} on the vertical axis, and the tectonic style of the frontal Jura represented with the colours defined on Figure 3. In cross-section A, for $\phi_{LC} \leq 4°$, the deformation propagates beyond the frontal part of the Jura and interferes with the Bresse graben. For $\phi_{LC} > 4°$, active tectonics is restricted to the southern part of the Jura or even further south, except as thin-skinned style if $\phi_{D_1} \leq 1°$ (or $\phi_{D_1} \leq 3°$ if $\phi_{LC} = 5°$). Moving eastward to cross-section B, the outcomes are similar, with slightly different threshold values (3° for ϕ_{LC} and 2° for ϕ_{D_1}). On cross-section C, the five tectonic styles appear for mere changes of ϕ_{LC} between 2° and 6° and ϕ_{D_1} between 4° and 5°. For $\phi_{D_1} \leq 4°$, D_1 is active and there is a thick-skinned style for $\phi_{LC} \leq 5°$, with small variations around these values. Eastward, to cross-sections D and E, the frontal part of the Jura never undergoes thin-skinned tectonics and ϕ_{D_1} appears to have a very little influence, only deciding whether D_1 is active on cross-section D (green/yellow limit). Note finally that in all cross-sections, the tectonic styles do not change, or change insignificantly, for values of ϕ_{D_1} or ϕ_{LC} greater than 8°. This justifies *a posteriori* the range of values investigated in this parametric analysis.

We can see in all graphs that ϕ_{D_1} determines if D_1 is active (blue and green together) or not (yellow), but it has little influence on the thick-skinned style (yellow and green together). By contrast, ϕ_{LC} controls the northern extent of the thick-skinned deformation and modulates subtly the activation of D_1. The sudden change from a thick-skinned front inside or to the south of the Jura (dark grey), to a front well beyond the folded Jura (light grey), upon minute changes of ϕ_{LC} is a striking outcome of this analysis.

The changes in these graphs from West to East suggest rather robustly that the frontal part of the Jura is not undergoing the same tectonic style everywhere. The western frontal part (prototype A) is more prone to thin-skinned tectonics, or to a thick-skinned tectonics that would emerge in the Bresse graben, while the eastern frontal part (cross-sections D and E), to thick-skinned tectonics emerging at the Jura front or beyond it.

4.3 Position of the thick-skinned front across the Jura belt

In order to have a synthetic view of the parametric analysis regarding the thick-skinned distribution, we draw the thick-skinned front of deformation across the Jura, interpolating it between the cross-sections (Fig. 5). To better visualise the outcrop of the front, we have blocked the Triassic décollement by setting $\phi_{D_1} = 10°$. Any area located to the north of this front is either submitted to thin-skinned deformation (not shown) or remains undeformed, depending on ϕ_{D_1}.

As expected, the lower is ϕ_{LC}, the further North and West propagates the thick-skinned front. For $\phi_{LC} \leq 2°$, the front is located beyond the Jura, for example reaching the Central massif (cross-section A), or the Vosges on section C (it corresponds to the light grey cases in Figs. 3 and 4). This seems rather unrealistic, at least in view of the quasi-absence of seismic activity in these regions. Seismic activity is however substantial in the Black Forest and Rhine graben parts (Rabin *et al.*, 2018), which are affected by thick-skinned deformation for $\phi_{LC} \leq 6°$ according to our map.

For $\phi_{LC} > 7°$, the thick-skinned front remains in the highest parts of the folded Jura near the border with the Molasse basin, except in sections D and E where it reaches the Jura front, or beyond (opaque dark grey region corresponding to ranges of $\phi_{LC} \leq 2°$ between 6 to 7° and 10°). Between 2° and 7°, the front progressively steps back toward the Alps in sections D and E, in contrast to sections A, B and C where it steps back in large sudden jumps (between 4° and 5° in section A and B, and between 2° and 3° in section C).

The lateral contrast of tectonic style in the Jura can be explained by the velocity fields of Figure 3; the more resistant is the lower crust (changing from 1° to 9°), the closer to the Alps outcrops the crustal ramp. The shape of the thick-skinned front therefore globally follows the shape of the Alps. In contrast, the shape of the Jura front is linked to the Triassic salt deposition area (Sommaruga, 1997), and therefore does not present the same curvature than the Alps. The eastern front of the Jura, closer to the Alps than the southern front, is therefore more likely to be submitted to thick-skinned tectonics. This general trend may also be influenced by the relief gap at the limit between the Jura Mountains and the Molasse basin, which is more pronounced in the southwest than in the northeast.

We conclude from these results that the eastern end of the Jura fold-and-thrust belt is always located to the South of

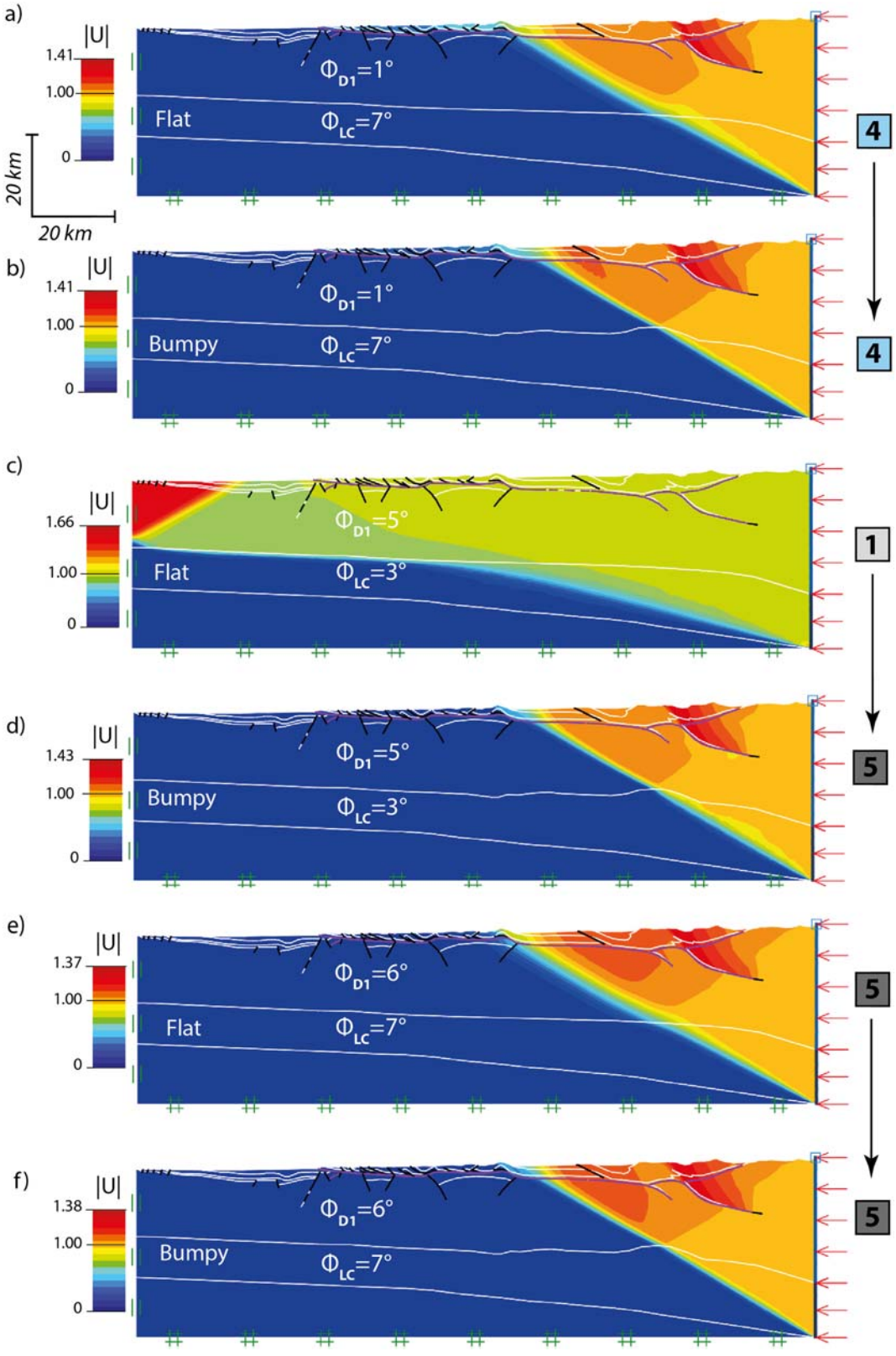

Fig. 6. Test of an irregular shape of the upper–lower crust limit on cross-section A. In (a), the case $\phi_{D_1} = 1°$, $\phi_{LC} = 7°$ initially corresponding to a thin-skinned style (blue region in the parametric study, Fig. 4) remains in the same tectonic style when setting a bumpy upper–lower crust limit in (b). In (c–d) and (e–f), same test, but for $\phi_{D_1} = 5°$, $\phi_{LC} = 3°$ and for $\phi_{D_1} = 6°$, $\phi_{LC} = 7°$, respectively. The case (c–d) shows a strong shift of tectonics from beyond the Jura in (c) to tectonics limited to the Molasse basin in (d).

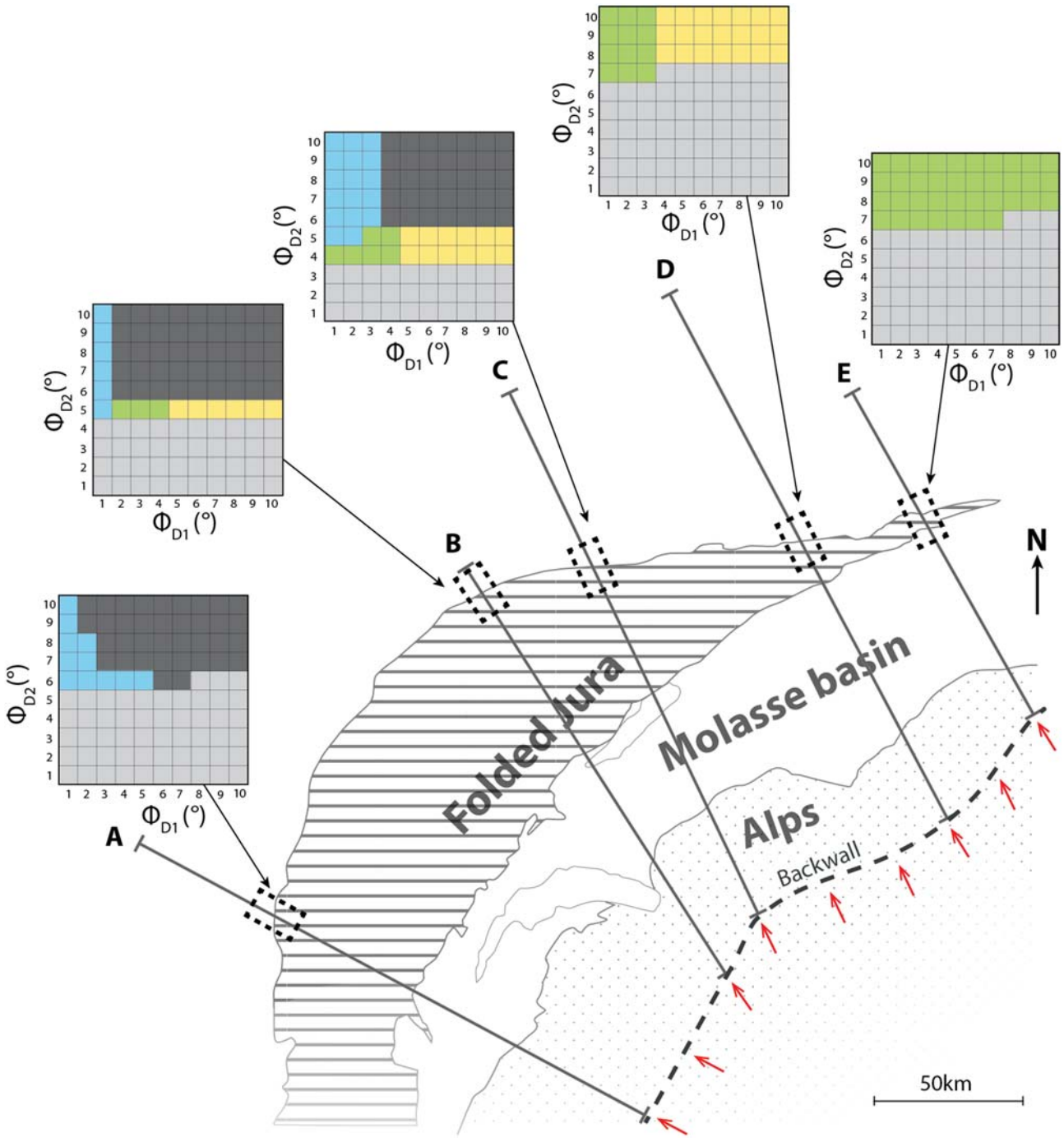

Fig. 7. Same legend as that of Figure 4. Here we use alternative cross-sections and boundary conditions (Fig. 2). The parameter ϕ_{LC} is replaced by the friction angle of the upper–lower crust interface ϕ_{D_2}.

the thick-skinned front, meaning that it undergoes currently thick-skinned tectonics, whatever the friction that we consider in the lower crust. In contrast, in the South-West, the front of the Jura is always located North-West of the thick-skinned front for $\phi_{LC} \geq 5°$, meaning that it undergoes currently thin-skinned tectonics, or none, since for $\phi_{LC} \leq 4°$, the thick-skinned deformation propagates too far to be supported by any existing data.

5 Discussion

5.1 Influence of the geometry and rheologies of the prototypes

The simple mechanical approach proposed in this study certainly makes strong simplifications on the rheology,

considering rigid-frictional Coulomb materials. This is relevant however to a situation where geological data is far too sparse and uncertain, in particular about the geometrical limits of the different materials, to conduct any precise modelling with the aim of a quantitative validation (Hindle and Kley, 2016). We nervertheless discuss a few factors mostly concerning the deep structure of the crust, which is not well known.

5.1.1 Shape of the upper–lower crust interface

The exact shape of the upper–lower crust interface is not constrained equally across the Jura belt. To the North-East, including the region of cross-section E, Rosenberg and Kissling (2013) draw a rather planar interface. It is only to the far East in the Engadine section that they propose thrusting in the lower crust that deforms the interface. However, Mock and Herwegh (2017), citing Pfiffner (2014), use the Conrad discontinuity corresponding to the $V_p = 6.5$ km/s isocontour as the interface, and draw it with undulations up to 10 km amplitude over several tens of kilometers around cross-section E. To the South-West, around our cross-section A, Pfiffner (2016) considers the same wavy pattern of the interface, again using the Conrad discontinuity as a guide. Since we consider different mechanical parameters for the upper and lower crust, the shape of the interface may well influence the location of the thrust crossing the crust. We show an example using cross-section A in Figure 6. For $\phi_{LC} = 7°$ (Fig. 6a–b and e–f), the bumpy interface does not change the position of the major thrust and the tectonic style at the surface remains unchanged, still controlled by the value of ϕ_{D_1}. However, for $\phi_{LC} = 3°$ (Fig. 6c–d), the bump in the interface captures the lower crust thrust, changing the tectonics from an activity beyond the folded Jura to an activity limited to the Molasse basin. Notice from the parametric analysis (Fig. 4, cross-section A) that the value $\phi_{LC} = 7°$ lies in the center of the dark grey area, while the value of 3° lies in the light grey area, but close to the limit with the dark grey area. It is therefore not surprising that this case is more sensitive to the shape of the interface.

5.1.2 Rheology of the upper–lower crust interface

In many cross-sections of orogenes, the upper crust forms stacked sheets showing that it is detached from the lower crust. Pfiffner (2016) remarks that the wavy shape of the upper–lower crust interface suggests an independent deformation of both parts. The hypothesis of a detachment at that interface was used by Lacombe and Mouthereau (2002) in their cross-sections of the Alps-Jura region. We have redone the parametric analysis of our cross-sections with two modifications: the tectonic push is now applied from the surface to the upper–lower crust limit only, and not down to the Moho, and, second, we fix the lower crust friction angle $\phi_{LC} = 10°$ and we introduce the friction angle of the interface, called ϕ_{D_2}, and let it vary in the same range: [1–10°] (see indications of Q_2 and D_2 in Fig. 2). The result (Fig. 7) is overall similar to the outcomes of the first analysis (Fig. 4). For the sections A, B and C, we only see minor quantitative shifts of the tectonic styles. In A, three styles can occur in the ranges $(\phi_{D_1}\ \phi_{LC}) = (3–4°,\ 4–5°)$, while in this new analysis they occur for $(\phi_{D_1}\ \phi_{D_2}) = (5–6°,\ 5–6°)$. In B, changes in styles occur for (4–5°, 3–4°), and all five styles may be found for (1–5°, 4–6°) in the new analysis, where additionnal styles appear only for $\phi_{D_2} = 5°$. In C, all five styles occur for (4–5°, 2–6°), and for (3–5°, 3–6°) in the new analysis. In D, again three styles occur for (3–4°, 7–8°), and for (3–4°, 6–8°) in the new analysis. In E, only two styles occur, largely independently of ϕ_{D_1}, and their limit is at $\phi_{LC} = 5–6°$ and $\phi_{D_2} = 6–8°$ in the new analysis (not shown on the graph, the décollement D_1 is blocked for $\phi_{D_1} \geq 20°$). Overall, the outcomes of the new analysis are very similar to those of the first analysis. The tectonic styles at the front of the Jura appear to be rather robust with respect to the application of the compression and to the response of the lower crust.

5.1.3 Intermediate décollement in the upper crust

The Permo-Carboniferous troughs underlying the Triassic décollement could root on some intermediate décollement within the upper crust (Lacombe and Mouthereau, 2002; Lacombe and Bellahsen, 2016). Such a décollement was inferred by cross-section balancing in the Jura mountains and the Molasse basin (Pfiffner, 2006) nearby our section C, where these troughs are currently reactivated in strike-slip mode (Mock and Herwegh, 2017). In Figure 8, we present a set of results on the section C with an additional décollement linking the deepest points of the Permo-Carboniferous normal faults under the Jura and the Molasse basin. We use the exact same five cases as those defining the tectonic styles (Fig. 3). In each case, we show the maximum value of the friction angle ϕ_{interm} of that intermediate décollement for which it is activated (the activation is hardly visible in the first case). Although these maximum values are low (2° for cross-sections A and E, and 4° for the others), they confirm the possibility to activate such a décollement if it is weak enough. If active, this intermediate décollement, located in the basement, implies a thick-skinned style, thus potentially changing the outcomes of the parametric analysis (Figs. 4 and 7). However, such a thick-skinned style is really only a variation of the thin-skinned style associated with the Triassic décollement. It does not involve the upper crust as substantially as the thick-skinned styles that we consider in our parametric analysis (Fig. 3, cases 2 and 3).

5.1.4 Effect of the cohesion

Recall that we chose cohesion values to ensure topographic stability of the outcropping units and that criterion yielded values from 1 to 1.5 MPa. Cohesion values could however be well above 1 MPa. To test the effect of higher cohesions, we have reproduced the parametric analysis of cross-section C using cohesion values of 5 MPa and 10 MPa for all rock units but the lower crust and mantle which stayed at 1 MPa (Fig. 9b, c). The comparison with the parametric study at 1 MPa (Fig. 9a) illustrates the effect of the cohesion. The thick-skinned style (green and yellow) is favored as it occurs for values of ϕ_{LC} up to 6° ($c = 5$ MPa, Fig. 9b) and 7° ($c = 10$ MPa, Fig. 9c) compared to the maximum value of 7° at $c = 1$ MPa (Fig. 9a). The lower limit on ϕ_{LC} below which deformation goes beyond the frontal Jura (ligh grey) remains unchanged. The slip on D_1, the Triassic décollement, is also favoured by the increase of cohesion as it occurs for values of ϕ_{D_1} below 5° at $c = 1$ MPa, 7°

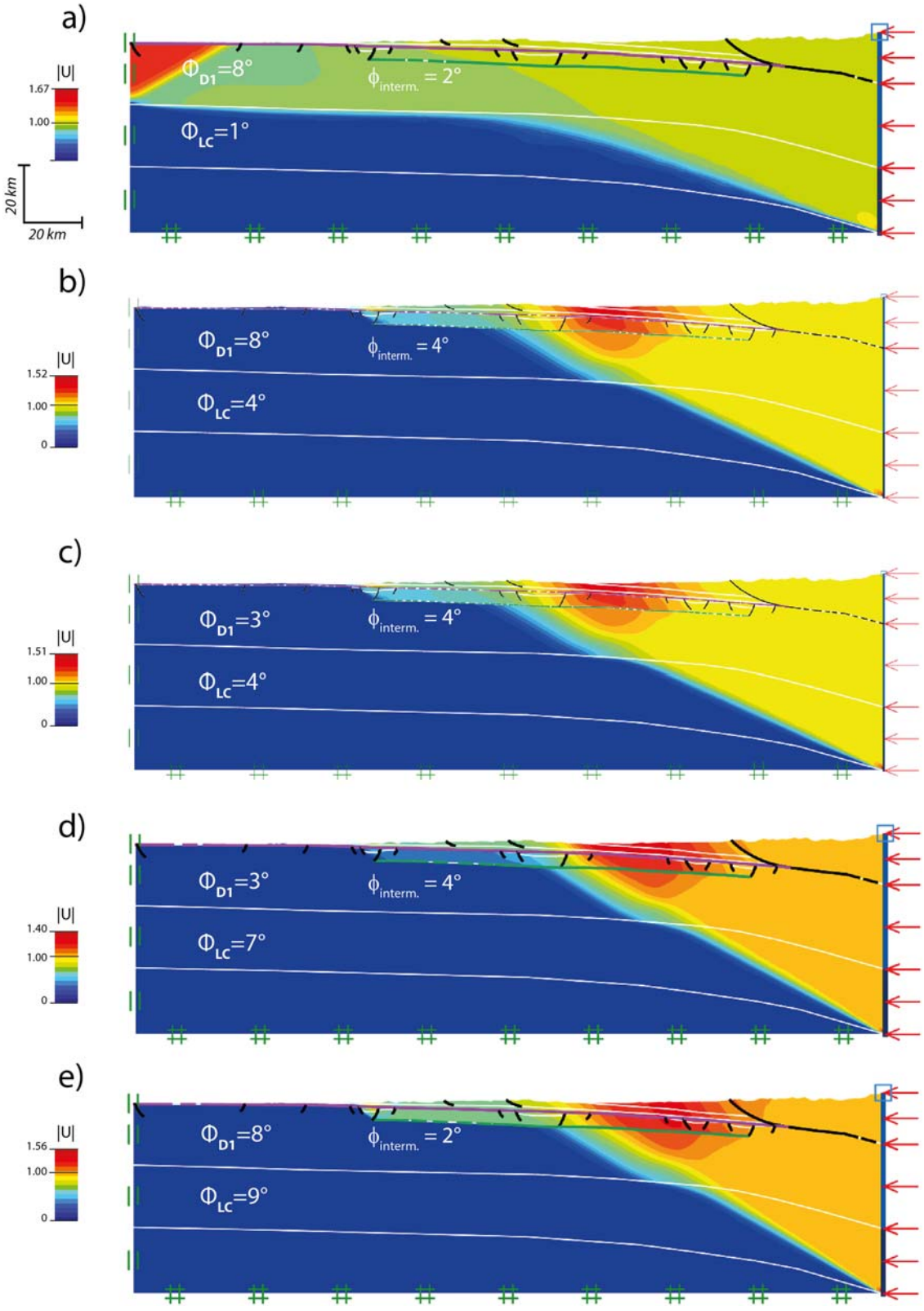

Fig. 8. Test of the effect of an additional intermediate décollement linking the Permo-Carboniferous troughs in cross-section C. From top to bottom, examples of the same cases as in Figure 3. We observe the activation of the intermediate décollement for any friction value ϕ_{interm} lower or equal to that indicated.

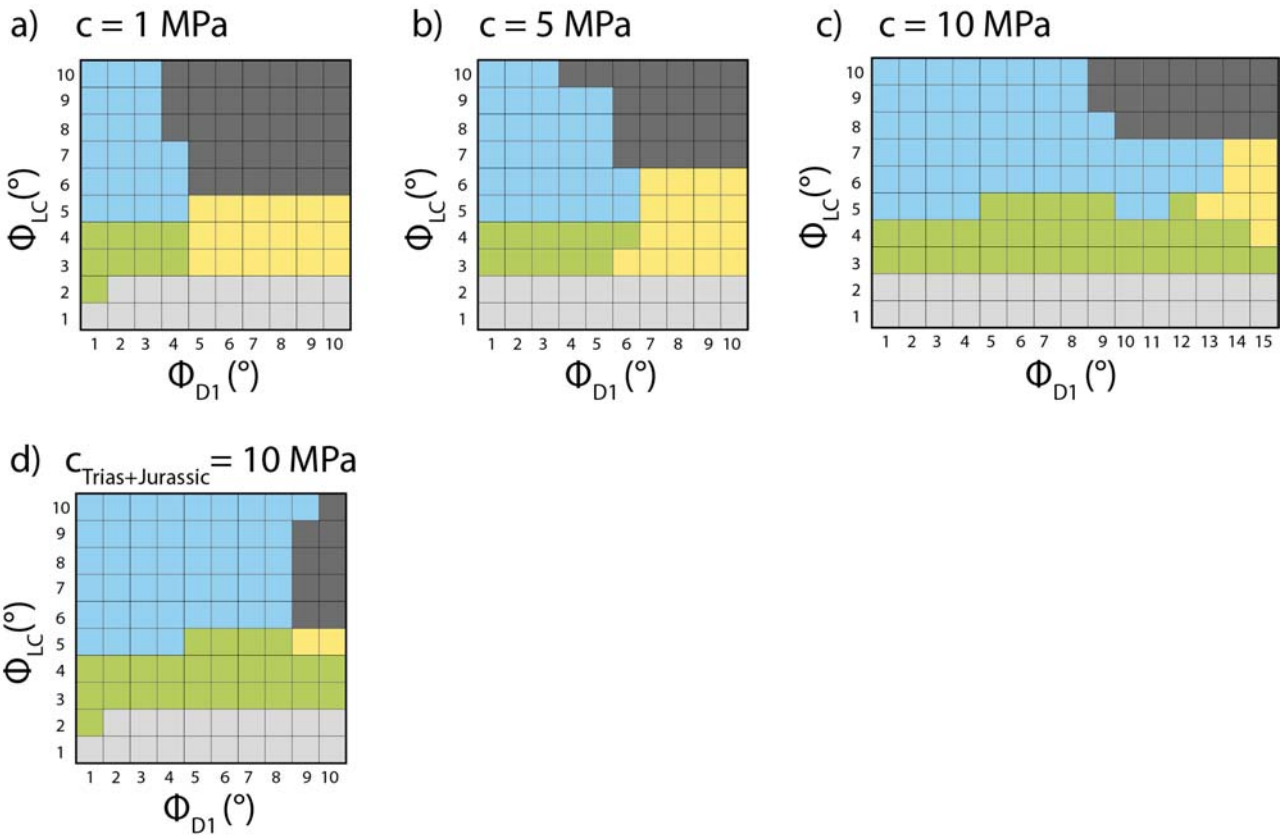

Fig. 9. Tectonic styles of cross-section C (same color code as in Fig. 3) for the cohesion value of the Jurassic, Triassic, Permo-Carboniferous and upper crustal rocks of 1 MPa (a), 5 MPa (b) and 10 MPa (c). In (d), only the cohesion of Jurassic and Triassic rocks is increased to 10 MPa. Note that (a) is reproduced from Figure 4 to facilitate comparison.

at $c = 5$ MPa, and about 14° at $c = 10$ MPa. The effect on the activation of D_1 is essentially due to the higher cohesion of the units above D_1 (Trias and Jurassic) as shown by the last test where only those rocks are more cohesive, the upper crust and Permo-Carboniferous rocks remaining at a cohesion of 1 MPa (Fig. 9d). Finally, it is worth noting that the limit between the four major tectonic styles of the frontal Jura (thin-skinned [blue], thick-skinned D_1 [green], thick-skinned [yellow], and no tectonics [dark grey]) remains within a narrow range of friction angles ϕ_{LC} and ϕ_{D_1}, although a bit less narrow. For a cohesion of 10 MPa, this range is shifted towards higher values of frictions, around 13° for ϕ_{D_1} and 5° to 8° for ϕ_{LC}. This observation is further discussed in Section 5.3.

The four questions discussed above imply complications that were not accounted for in our simple analysis of only two parameters (ϕ_{D_1} and ϕ_{LC}). They can be adressed, as demonstrated, but at the cost of more complex prototypes and more parameters. They suggest that several solutions (in terms of structure and rheology) are possible when comparing the numerical outcomes to geological interpretations of field data, and to the GPS data, hypocenters and focal mechanisms recently gathered and presented by Rabin *et al.* (2018).

5.2 Occurrence of thick-skinned tectonics

The question of the current tectonic style of the Jura fold-and-thrust belt is debated, since arguments for activation of the basement but also arguments for an activation of the Triassic décollement exist, and these arguments distinguish the NE and SW ends of the Jura.

Using natural seismicity and GPS data, Rabin *et al.* (2018) observe a strong contrast of tectonic style between the North-East part of the Jura and the Central and South-West parts. They show that most earthquakes in the North-East are strike-slip with NNW–SSE main compression and at depths between 15 and 30 km implying a thick-skinned style involving the whole crust. They further infer basement–cover decoupling in the NE from the GPS data. In contrast, the Central and South parts develop much less earthquakes, and at depths between 0 and 10 km. Focussed on the Rhine-Bresse transfer zone in the NW front of the Jura belt (around our cross-sections B and C), Madritsch *et al.* (2008) conclude from field, well and seismic data that this region is currently, and since post-early Pliocene times, undergoing thick-skinned tectonics in strike-slip mode by reactivation of normal faults of the transfer zone, with a simultaneous activation of the Triassic décollement in places.

Re-interpreting seismic data in the Molasse basin to the West of our cross-section D, Mock and Herwegh (2017) also conclude on a current transition toward a thick-skinned style in this region with Permo-Carboniferous normal faults reactivated in strike-slip mode down to depths of 30 km.

Our parametric analysis is compatible with these observations and interpretations of the current evolution toward thick-skinned tectonics that is more advanced in the NE and probably not yet started in the SW. The uniformity of the GPS data in the NE region comprising the folded Jura and the Molasse basin is compatible with a thick-skinned tectonics that emerges North of the Jura front (Fig. 5 for $\phi_{LC} \leq 7°$, sections D and E). Also, the basement–cover decoupling in the NE (Rabin *et al.*, 2018) corresponds to the occurence of the green style on cross-sections D and E (Figs. 4 and 7). Also, for values of $\phi_{LC} \leq 3$ to 5° in the sections B and C (Figs. 4 and 7), we retrieve the thick-skinned mode observed in the Rhine-Bresse transfer zone, with activation of the Triassic décollement for $\phi_{D_1} \leq 4°$ in cross-section B. The numerical outcomes also suggest a lateral change from a thick-skinned to a thin-skinned style from the North-East to the South-West of the Jura. Indeed, whatever the friction values we consider for ϕ_{D_1} and ϕ_{LC}, the frontal part of the northeastern Jura undergoes thick-skinned tectonics while the southwestern frontal part of the Jura undergoes thin-skinned tectonics, or is passively transported on a deep crustal thrust that would interfere with the Bresse graben ($\phi_{LC} \leq 4°$), or it undergoes no activity at all ($\phi_{LC} \geq 5°$, Figs. 4 and 5).

5.3 Criticality

Our results show that a thin-skinned activation of all the Jura front requires a very low friction angle on the Triassic décollement: less than 2° in the West and up to 4° in the North-East (Fig. 4) (except in cross-section E where the décollement is active at least up to 10°). This result is in very good agreement with the critical taper analysis of the Triassic décollement in the Jura and the Alps of Von Hagke *et al.* (2014); they estimated very low frictions, less than 3° for the evaporites.

However, the challenge here is to go beyond the wedge geometry imposed by the Critical Coulomb Wedge (CCW) theory (Davis *et al.*, 1983). In that respect, the limit analysis method, with its frictional materials, is a theoretical and numerial generalisation of the CCW theory, which allows us to consider the deeper parts of the Jura and investigate thick-skinned tectonics. In doing so we had to choose surrounding material properties and structures far away from the Jura, which are not very well constrained. Overall, the tests presented in Figures 6, 7 and 8, show that not only ϕ_{D_1} and ϕ_{LC}, but also that the shape of the upper–lower crust, its rheology, or an intermediate décollement in the upper crust can all be triggering parameters for a change in tectonic style. Another striking feature of the outcomes of our analyses is the sudden change between different tectonic styles for minute changes in the values of ϕ_{D_1} and ϕ_{LC} (Fig. 4). This observation remains for all the range of possible cohesion values (Fig. 9). These two remarks suggest the existence of a critical state much in the sense of the CCW theory corresponding to a narrow range in various parameters of the prototypes where several distinct tectonic solutions may occur (Cubas *et al.*, 2008; Mary *et al.*, 2013a). The stable state corresponds to the tectonic type 1, where deformation goes beyond the Jura front, and the unstable states to cases 2, 3, 4, and 5 (Fig. 3). The critical states, indicated by the zones of changes of colour in the graphs of Figure 4, are thus enriched compared to the CCW theory, even though we tested only two parameters in order to keep the spirit of simplicity of the CCW approach.

6 Conclusion

We give a mechanical point of view using the limit analysis theory on the question of the current tectonic style in the Jura belt by varying the friction angles of the Triassic décollement and of the lower crust. We have pushed here limit analysis beyond its strict limit of applicability since we model the lower crust as a frictional Coulomb material rather than a ductile, temperature- and rate-dependent material. It is an exploration of mechanical solutions that complements the "all ductile" approach of many numerical implementations concerned with lithospheric scale tectonics but meeting difficulties at the scale of individual faults in the upper crust. Despite the approximate rheology used here and the simplicity of the prototypes (isotropic, homogeneous crust, in two dimensions), we capture important features of the tectonics by determining friction values compatible with incipient thick-skinned tectonics and its lateral variations from NE to SW. By classifying the results in terms of the tectonics affecting the front of the folded Jura, the main conclusions can be listed in three points:

- we show that all the Jura is not undergoing the same tectonic style, the thick-skinned front of deformation indeed separates the northeastern Jura from the southwestern Jura. This is due to the fact that the thick-skinned front of deformation follows the curvature of the Alps, which is not the same than that of the Jura belt. While the oriental termination of the Jura belt undergoes thick-skinned tectonics whatever the friction values that we consider, the southwestern Jura front on the contrary is never reached by the thick-skinned front, which emerges either in the central or high Jura, or far away in the Bresse graben;
- the thick-skinned tectonics affecting the oriental termination of the Jura can however be accompanied by a simultaneous activation of the Triassic décollement;
- overall, our conclusions are compatible with published focal mechanisms, earthquake data, GPS data for a friction angle of the lower crust around 6° in the North-East and 3° to 4° in the Central area. It is less well constrained in the South-West area. The activation of the Triassic décollement occurs for friction values below 5° (except in the extreme North-East), with precise limits changing across the Jura.

This study shows more generally that the tectonics in the Alpine foreland is governed by a threshold phenomenon with different tectonic styles depending on the rheological and geometrical sets of parameters. Similarly to the Critical Coulomb Wedge theory, if the entire prototype is in a critical state, then different tectonics styles can occur for a very narrow range of parameter values.

Allowing for uncertainties in the large scale structures, boundary conditions and rheology, the tectonic styles affecting the Jura remain the same, although they may occur for different

values of the friction coefficients. More complex simulations accounting for the three dimensions, complex rheologies and inherited structures should come in the future and the present work may serve as a first approximation of the modelling of the current active structures.

Acknowledgments. We are grateful to CY Cergy Paris Université for the financing of Typhaine Caër's PhD, and to swisstopo for the financial support of the work presented in this paper. We also address our thanks to Yves Leroy and Sylvain Calassou for their useful advices, and to Adrian Pfiffner and Artur Bauville for their reviews of an earlier version of this article.

References

Affolter T, Gratier J-P. 2004. Map view retrodeformation of an arcuate fold-and-thrust belt: the jura case. *Journal of Geophysical Research: Solid Earth* 109: b03404.

Baize S, Cushing M, Lemeille F, Granier T, Grellet B, Carbon D, *et al.* 2002. Inventaire des indices de rupture affectant le quaternaire, en relation avec les grandes structures connues, en France métropolitaine et dans les régions limitrophe. *Mémoires de la Société géologique de France* 175: 1–141.

Bauville A, Schmalholz SM. 2015. Transition from thin- to thick-skinned tectonics and consequences for nappe formation: numerical simulations and applications to the Helvetic nappe system, Switzerland. *Tectonophysics* 665: 101–117.

Becker A. 2000. The Jura Mountains – an active foreland fold-and-thrust belt! *Tectonophysics* 321: 381–406.

Buiter S, Babeyko AY, Ellis S, Gerya TV, Kaus BJ, Kellner A, *et al.* 2006. The numerical sandbox: comparison of model results for a shortening and an extension experiment, vol. 253. The Geological Society of London Special Publication, pp. 29–64.

Buiter SJ, Schreurs G, Albertz M, Gerya TV, Kaus B, Landry V, *et al.* 2016. Benchmarking numerical models of brittle thrust wedges. *Journal of Structural Geology* 92: 140–177.

Burkhard M. 1990. Aspects of the large-scale miocene deformation in the most external part of the Swiss Alps (sub-alpine molasse to jura fold belt). *Eclogae Geologicae Helvetiae* 83: 559–583.

Burkhard M, Sommaruga A. 1998. Evolution of the western Swiss molasse basin: structural relations with the Alps and the jura belt. In: Mascle A, Puigdefabregas C, Luterbacher H, Fernandez M, eds. Cenozoic foreland basins of Western Europe, vol. 134. Geological Society Special Publications, pp. 279–298.

Buxtorf A. 1916. Prognosen und Befunde beim Hauensteinbasis-und Grenchenbergtunnel und die Bedeutung der letztern für die Geologie des Juragebirges, vol. 27. E. Birkhauser.

Caër T, Souloumiac P, Maillot B, Leturmy P, Nussbaum C. 2018. Propagation of a fold-and-thrust belt over a basement graben. *Journal of Structural Geology* 115: 121–131.

Chapple VM. 1978. Mechanics of thin-skinned fold-and-thrust belts. *Geological Society of America Bulletin* 89: 1189–1198.

Costa E, Vendeville B. 2002. Experimental insights on the geometry and kinematics of fold-and-thrust belts above weak, viscous evaporitic décollement. *Journal of Structural Geology* 24: 1729–1739.

Cubas N, Leroy YM, Maillot B. 2008. Prediction of thrusting sequences in accretionary wedges. *Journal of Geophysical Research* 113: 1–21.

Dahlen FA. 1984. Noncohesive critical Coulomb Vedges: an exact solution. *Journal of Geophysical Research* 89: 10125–10133.

Davis D, Suppe J, Dahlen FA. 1983. Mechanics of fold-and-thrust belts and accretionary vedges. *Journal of Geophysical Research* 88: 1153–1172.

De La Taille C. 2015. Évalutation de l'activité tectonique quaternaire des failles du jura méridional (France). Ph.D. thesis. Université de Grenoble Alpes.

Deichmann N, Dolfin DB, Kastrup U. 2000. Seismizitat der Nord-und Zentralschweiz: Dezember 2000. Nagra.

Dreyfuss M, Glangeaud L. 1950. La vallée du Doubs et l évolution morphotectonique de la région bisontine.

Ferry M, Meghraoui M, Delouis B, Giardini D. 2005. Evidence for holocene palaeoseismicity along the basel-reinach active normal fault (Switzerland): a seismic source for the 1356 earthquake in the upper rhine graben. *Geophysical Journal International* 160: 554–572.

Giamboni M, Ustaszewski K, Schmid S, Schumacher M, Vetzel A. 2004. Plio-pleistocene trans-pressional reactivation of paleozoic and paleogene structures in the rhine-bresse transform zone (northern Switzerland and eastern France). *International Journal of Earth Sciences* 93: 207–223.

Guellec S, Mugnier J-L., Tardy M, Roure F. 1990. Neogene evolution of the western alpine foreland in the light of ecors data and balanced cross-section. *Mémoires de la Société géologique de France* 156: 165–184.

Hindle D, Kley J. 2016. Modelling "reality" in tectonics: simulation of the mechanical evolution of the jura mountains-molasse basin system, and routes to forward-inverse modelling of fold thrust belts. In: EGU General Assembly Conference Abstracts, pp. EPSC2016–10470.

Homberg C. 1997. Analyse des déformations cassantes dans le jura et modélisation numérique des perturbations des contraintes tectoniques autour d'accidents majeurs. Ph.D. thesis.

Humair F, Bauville A, Epard J-L., Schmalholz SM. 2020. Interaction of folding and thrusting during fold-and-thrust-belt evolution: Insights from numerical simulations and application to the Swiss jura and the Canadian foothills. *Tectonophysics* 789: 228474.

Jammes S, Huismans RS. 2012. Structural styles of mountain building: controls of lithospheric rheologic stratification and extensional inheritance. *Journal of Geophysical Research: Solid Earth* 117.

Jammes S, Huismans RS, Mufioz JA. 2014. Lateral variation in structural style of mountain building: controls of rheological and rift inheritance. *Terra Nova* 26: 201–207.

Jaquet Y, Bauville A, Schmalholz SM. 2014. Viscous overthrusting *versus* folding: 2-d quantitative modeling and its application to the helvetic and jura fold and thrust belts. *Journal of Structural Geology* 62: 25–37.

Jordan P. 1992. Evidence for large-scale decoupling in the triassic evaporites of northern Switzerland: an overview. *Eclogae Geologicae Helvetiae* 85: 677–693.

Jouanne F, Ménard G, Jault D. 1994. Present-day deformation of the french northwestern alps/southern jura mountains: comparison between historical triangulations. *Geophysical Journal International* 119: 151–165.

Kastrup U, Zoback ML, Deichmann N, Evans KF, Giardini D, Michael AJ. 2004. Stress field variations in the Swiss Alps and the northern Alpine foreland derived from inversion of fault plane solutions. *Journal of Geophysical Research: Solid Earth* 109.

Krabbenhøft K, Damkilde L. 2003. A general non-linear optimization algorithm for lower bound limit analysis. *International Journal for Numerical Methods in Engineering* 56: 165–184.

Krabbenhøft K, Lyamin AV, Optum G2. 2014. Optum computational engineering. www.optumce.com.

Krabbenhøft K, Lyamin AV, Hjiaj M, Sloan SV. 2005. A new discontinuous upper bound limit analysis formulation. *International Journal for Numerical Methods in Engineering* 63: 1069–1088.

Lacombe O, Bellahsen N. 2016. Thick-skinned tectonics and basement-involved fold-thrust belts: insights from selected cenozoic orogens. *Geological Magazine* 153: 763–810.

Lacombe O, Mouthereau F. 2002. Basement-involved shortening and deep detachment tectonics in forelands of orogens: insights from recent collision belts (Taiwan, western Alps, Pyrenees). *Tectonics* 21: 12–1.

Lambert J, Vinter T, Dewez TJ, Sabourault P. 2005. New hypotheses on the maximum damage area of the 1356 Basel earthquake (Switzerland). *Quaternary Science Reviews* 24: 381–399.

Lanza F, Diehl T, Deichmann N, Kraft T, Nussbaum C, Schefer S, *et al.* 2022. The saint-ursanne earthquakes of 2000 revisited: evidence for active shallow thrust-faulting in the jura fold-and-thrust belt. *Swiss Journal of Geosciences* 115: 1–24.

Laubscher H. 1992. Jura kinematics and the molasse bassin. *Eclogae Geologicae Helvetiae* 85: 653–675.

Laubscher HP. 1961. Die fernschubhypothese der jurafaltung. *Eclogae Geologicae Helvetiae* 54: 222–282.

Lyamin AV, Sloan SV, Krabbenhøft K, Hjiaj M. 2005. Lower bound limit analysis with adaptive remeshing. *International Journal for Numerical Methods in Engineering* 63: 1961–1974.

Madritsch H. 2008. Structural evolution and neotectonics of the rhine-bresse transfer zone. Ph.D. thesis. University of Basel.

, Madritsch H, Schmid SM, Fabbri O. 2008. Interactions between thin-and thick-skinned tectonics at the northwestern front of the jura fold-and-thrust belt (eastern France). *Tectonics* 27.

Madritsch H, Preusser F, Fabbri O, Bichet V, Schlunegger F, Schmid SM. 2010. Late quaternary folding in the jura mountains: evidence from syn-erosional deformation of fluvial meanders. *Terra Nova* 22: 147–154.

Maillot B, Leroy YM. 2006. Kink-fold onset and development based on the maximum strength theorem. *Journal of the Mechanics and Physics of Solids* 54: 2030–2059.

Mary B, Maillot B, Leroy YM. 2013a. Deterministic chaos in frictional wedges revealed by convergence analysis. *Int J Numer Anal Meth Geomech*.

Mary B, Maillot B, Leroy YM. 2013b. Predicting orogenic wedge styles as a function of analogue erosion law and material softening. *Geochemistry, Geophysics, Geosystems* 14.

Mary BCL. 2012. Au-delà du prisme critique de Coulomb par l'analyse limite séquentielle et contributions expérimentales. Doctoral thesis. France: Université de Cergy-Pontoise.

Meghraoui M, Delouis B, Ferry M, Giardini D, Huggenberger P, Spottke I, *et al.* 2001. Active normal faulting in the upper rhine graben and paleoseismic identification of the 1356 Basel earthquake. *Science* 293: 2070–2073.

Meyer B, Lacassin R, Brulhet J, Mouroux B. 1994. The Basel 1356 earthquake: which fault produced it! *Terra Nova* 6: 54–63.

Mock S, Herwegh M. 2017. Tectonics of the central swiss molasse basin: post-miocene transition to incipient thick-skinned tectonics! *Tectonics* 36: 1699–1723.

Mosar J. 1999. Present-day and future tectonic underplating in the western swiss alps: reconciliation of basement wrench-faulting and decollement folding of the Jura and Molasse basin in the alpine foreland. *Earth and Planetary Science Letters* 173: 143–155.

Mugnier J, Vialon P. 1986. Deformation and displacement of the jura cover on its basement. *Journal of Structural Geology* 8: 373–387.

Nivière B, Winter T. 2000. Pleistocene northwards fold propagation of the jura within the southern upper rhine graben: seismotectonic implications. *Global and Planetary Change* 27: 263–288.

Nussbaum C, Bossart P, Amann F, Aubourg C. 2011. Analysis of tectonic structures and excavation induced fractures in the opalinus clay, Mont Terri underground rock laboratory (Switzerland). *Swiss Journal of Geosciences* 104: 187–210.

Nussbaum C, Kloppenburg A, Caër T, Bossart P. 2018. Tectonic evolution around the mont terri rock laboratory, northwestern Swiss jura: constraints from kinematic forward modelling. In: Mont Terri Rock Laboratory, 20 years. Springer, pp. 41–68.

Pfiffner OA. 2014. Geology of the Alps. Wiley.

Pfiffner OA, Erard P, Stauble M. 1997. Two cross-sections through the Swiss Molasse basin (lines e4-e6, w1, w7-w10). *Deep structure of the Swiss Alps. Results of NRP* 20: 64–72.

Pfiffner OA. 2006. Thick-skinned and thin-skinned styles of continental contraction. *Geological Society of America Special Papers* 414: 153–177.

Pfiffner OA. 2016. Basement-involved thin-skinned and thick-skinned tectonics in the Alps. *Geological Magazine* 153: 1085–1109.

Pfiffner OA, Klaper EM, Mayerat A-M, Heitzmann P. 1990. Structure of the basement-cover contact in the Swiss Alps. *Mémoires de la Société géologique de France* 156: 247–262.

Philippe Y. 1995. Rampes latérales et zones de transfert dans les chaînes plissées: géométrie, condition de formation et pièges structuraux associés. Ph.D. thesis. Université de Savoie.

Rabin M, Sue C, Valpersdorf A, Sakic P, Albaric J, Fores B. 2018. Present-day deformations of the jura arc inferred by gps surveying and earthquake focal mechanisms. *Tectonics* 37: 3782–3804.

Radaideh OM, Mosar J. 2021. Cenozoic tectonic deformation along the pontarlier strike-slip fault zone (Swiss and French jura fold-and-thrust belt): insights from paleostress and geomorphic analyses. *Tectonics* 40: e2021TC006758.

Rodgers J. 1949. Evolution of thought on structure of middle and southern appalachians. *AAPG Bulletin* 33: 1643–1654.

Rosenberg CL, Kissling E. 2013. Three-dimensional insight into central-alpine collision: lower-plate or upper-plate indentation! *Geology* 41: 1219–1222.

Rotstein Y, Schaming M. 2004. Seismic reflection evidence for thick-skinned tectonics in the northern jura. *Terra Nova* 16: 250–256.

Rotstein Y, Edel J-B, Gabriel G, Boulanger D, Schaming M, Munschy M. 2006. Insight into the structure of the upper rhine graben and its basement from a new compilation of bouguer gravity. *Tectonophysics* 425: 55–70.

Ruh JB, Le Pourhiet L, Agard P, Burov E, Gerya T. 2015. Tectonic slicing of subducting oceanic crust along plate interfaces: numerical modeling. *Geochemistry, Geophysics, Geosystems* 16: 3505–3531.

Salençon J. 1974. Théorie de la plasticité pour les applications à la mécanique des sols (English translation: Application of the theory of plasticity in soil mechanics. New York: Wiley, 1977). Paris: Eyrolles.

Salençon J. 2002. De l'élasto-plasticité au calcul à la rupture. Palaiseau: École Polytechnique, and Paris: Ellipses.

Schmid S, Kissling E. 2000. The arc of the western alps in the light of geophysical data on deep crustal structure. *Tectonics* 19: 62–85.

Schori M. 2021. The development of the jura fold-and-thrust belt: pre-existing basement structures and the formation of ramps. Ph.D. thesis. Switzerland: University of Fribourg.

Schori M, Zwaan F, Schreurs G, Mosar J. 2021. Pre-existing basement faults controlling deformation in the jura mountains fold-and-thrust belt: insights from analogue models. *Tectonophysics* 814: 228980.

Sommaruga A. 1997. Geology of the central jura and the molasse basin: new insight into an evaporite-based foreland fold and thrust belt. *Mem. 12. Paris: Soc. des Sci. Nat. de Neuchatel*, 176 p.

Sommaruga A. 1999. Décollement tectonics in the jura foreland fold-and-thrust belt. *Marine and Petroleum Geology* 16: 111–134.

Sommaruga A, Eichenberger U, Marillier F, Kissling E. 2012. Seismic atlas of the Swiss molasse basin.

Souloumiac P. 2009. Mécanismes 3d de ruine en géologie structurale: approche numérique et analogique. Ph.D. thesis. École Centrale de Paris.

Souloumiac P, Leroy YM, Krabbenhøft K, Maillot B. 2009. Predicting stress in fault-bend fold by optimization. *J Geophys Res* 114: B09404.

Souloumiac P, Krabbenhøft K, Leroy YM, Maillot B. 2010. Failure in accretionary wedges with the maximum strength theorem: numerical algorithm and 2D validation. *Computational Geosciences*.

Strayer LM, Hudleston PJ, Lorig LJ. 2001. A numerical model of deformation and fluid-flow in an evolving thrust wedge. *Tectonophysics* 335: 121–145.

Ustaszewski K, Schmid SM. 2006. Control of preexisting faults on geometry and kinematics in the northernmost part of the jura fold-and-thrust belt. *Tectonics* 25.

Ustaszewski K, Schmid SM. 2007. Latest pliocene to recent thick-skinned tectonics at the upper rhine graben-jura mountains junction. *Swiss Journal of Geosciences* 100: 293–312.

Ustaszewski K, Schumacher ME, Schmid SM, Nieuwland D. 2005. Fault reactivation in brittle-viscous wrench systems-dynamically scaled analogue models and application to the rhine-bresse transfer zone. *Quaternary Science Reviews* 24: 363–380.

Von Hagke C, Oncken O, Evseev S. 2014. Critical taper analysis reveals lithological control of variations in detachment strength: an analysis of the alpine basal detachment (Swiss Alps). *Geochemistry, Geophysics, Geosystems* 15: 176–191.

Wissing S, Ellis S, Pfiffner O. 2003. Numerical models of alpine-type cover nappes. *Tectonophysics* 367: 145–172.

Cite this article as: Caër T, Maillot B, Leturmy P, Souloumiac P, Nussbaum C. 2023. Parametric mechanical analysis of thin- *versus* thick-skinned tectonics applied to the Jura belt, *BSGF - Earth Sciences Bulletin* 194: 5.